



DEGREE PROJECT IN MEDICAL ENGINEERING,
SECOND CYCLE, 30 CREDITS
STOCKHOLM, SWEDEN 2018

Smartphone Acquisition and Online Visualization of IMU and EMG Sensor Data for Assessment of Wrist Load

**Smartphone-mätning och online-
visualisering av IMU- och EMG-data
för bedömning av
handledsbelastning**

DANIEL MUNGUIA CHANG & AXEL HULT

KTH ROYAL INSTITUTE OF TECHNOLOGY
SCHOOL OF ENGINEERING SCIENCES IN CHEMISTRY,
BIOTECHNOLOGY AND HEALTH

Abstract

Work-related musculoskeletal disorders constitutes a substantial burden for society, generating individual suffering and financial costs. Quantifying the musculoskeletal stress and establishing exposure-response relationships is an important step in facing this problem.

Observational methods for assessing exposure in the field of ergonomics have shown poor results, and the technical measurement methods that exists are often complicated to use which limits their scope to scientific purposes.

This work describes the development of a prototype measurement system aimed to simplify ambulatory measurements of musculoskeletal load, specifically aimed at the wrist and hand. Wearable sensors including Inertial Measurement Units (IMU:s) and Electromyography (EMG) were connected to a smartphone and used for measuring wrist movement and forearm muscle activity. Data sampled in the smartphone was stored online in a cloud database, and a web-application was developed to visualize work-load exposure.

Testing under controlled conditions indicated that muscular rest can be measured and classified according to suggested risk thresholds. Accurate angular measurements were difficult to implement because of lacking inter-sensor alignment in the horizontal plane, as well as uncertainties in the Bluetooth protocol.

Future work should focus on the IMU:s and look to further develop a method of correcting the relative angle error, as well as investigating accurate time synchronization of the two sensors. Alternatively, deriving angular velocities directly from the IMU gyroscopes could be investigated.

Keywords: Wrist, Work-related musculoskeletal disorders, WRMD, Inertial Measurement Unit, IMU, Electromyography, EMG, Goniometer

"The scientific man does not aim at an immediate result. He does not expect that his advanced ideas will be readily taken up. His work is like that of the planter — for the future. His duty is to lay the foundation for those who are to come, and point the way."

Nikola Tesla

Content

Acronyms and Abbreviations	vi
List of Figures	vii
List of Tables	viii
1. Introduction	1
1.1. Background.....	1
1.2. Purpose and Goals	2
2. Materials and Method.....	3
2.1. IMU.....	3
2.1.1. System Description.....	3
2.1.2. Motion Drift	4
2.1.3. Magnetic Field Environment Test.....	4
2.1.4. Static Angles Test.....	5
2.1.5. Dynamic Angle Test.....	5
2.2. EMG.....	6
2.2.1. System Description.....	6
2.2.2. EMG Signal Processing	6
2.2.3. EMG Amplitude Test.....	7
2.2.4. Re-alignment Algorithm	7
2.3. Data storage and visualization.....	10
2.3.1. Database and Data Modelling	10
2.3.2. Data Visualization	10
3. Results	11
3.1. IMU.....	11
3.1.1. Motion drift.....	11
3.1.2. Magnetic Field Environment Test.....	12
3.1.3. Static Angles Test.....	13
3.1.4. Dynamic Angles Test.....	14
3.2. EMG.....	16
3.2.1. EMG Signal Processing	16
3.2.2. EMG Amplitude Test.....	16
3.2.3. Re-alignment Algorithm	19
3.3. Data storage and visualization.....	20
3.3.1. Android application.....	20

3.3.2. Web application	20
4. Discussion.....	22
5. Conclusion	25
References	26

Appendix A: State of the Art Report

Appendix B: LPMS-B2 Datasheet

Appendix C: Shimmer3 Datasheet

Appendix D: Additional test data

Acronyms and Abbreviations

EMG	<i>Electromyography</i>
IMU	<i>Inertial Measurement Unit</i>
KI IMM	<i>Karolinska Institute, Institute of Environmental Medicine</i>
MVC	<i>Maximum Voluntary Contraction</i>
MVE	<i>Maximum Voluntary Electrical Activation</i>
rms-EMG	<i>Root-mean-square of an electromyography signal</i>
RMSE	<i>Root-mean-square-error</i>
WRMD	<i>Work-Related Musculoskeletal Disorder</i>

List of Figures

Figure 1.1: Measurement technology used in ergonomics	1
Figure 2.1: Rotations as quaternions	3
Figure 2.2: Magnetic field environment test setup	4
Figure 2.3: Test-setup for simulated screw-sorting task	5
Figure 2.4: EMG and IMU:s	7
Figure 2.5: Flowchart of the re-alignment algorithm	8
Figure 2.6: Re-alignment algorithm test setup	9
Figure 2.7: Modeling sensor data in MongoDB	10
Figure 3.1: Motion generated drift	11
Figure 3.2: Environmental test, with magnetometer	12
Figure 3.3: Environmental test, without magnetometer	12
Figure 3.4: Bland-Altman plot, pitch rotation	13
Figure 3.5: Bland-Altman plot, yaw rotation	13
Figure 3.6: Wrist extension/flexions at 30 BPM	14
Figure 3.7: Angular velocity distribution (first repetition)	15
Figure 3.8: Angular velocity distribution (second repetition)	15
Figure 3.9: EMG signal-processing sample distributions	16
Figure 3.10: EMG-amplitudes from contraction test	17
Figure 3.11: EMG-amplitudes from contraction test, last repetition	17
Figure 3.12: Wrist and muscular activity during loaded flexion/extension	18
Figure 3.13: Re-alignment algorithm test	19
Figure 3.14: Interface for the Android application	20
Figure 3.15: Interface for the Web application	21

List of Tables

Table 2.1: Development overview	3
Table 2.2: EMG-filters and coefficients	6
Table 2.3: Parameters in re-alignment algorithm	7
Table 2.4: Parameter-limits used for re-alignment test	9
Table 2.5: RMSE of angles from dynamic angle test	14
Table 2.6: RMSE of angular velocities from dynamic angle test	14
Table 2.7: Angular velocity in percentiles (first repetition)	15
Table 2.8: Angular velocity in percentiles (second repetition)	16

1. Introduction

Sustaining healthy and ergonomic working environments can be a crucial step in maintaining employee wellbeing and efficiency. Work-related injuries and sickness can otherwise create a continuous expense in the form of worker absence, healthcare costs and most importantly human suffering. In the UK alone, 137 million working days were reported lost in 2016 due to injuries and sickness, among which, Work-Related Musculoskeletal Disorders (WRMD:s) were the most common causes [1].

WRMDs are defined as disorders concerning muscles, nerves, tendons, ligaments, and joints. Studies have classified wrist and hand injuries internationally as one of the most prominent WRMDs [1] [2] [3], raising awareness and need for preventive actions. However, this requires us to first comprehend the extent in which wrists and hands are used in various occupations and working environments.

1.1. Background

Observational methods used by ergonomists can produce low-reliability and inaccurate estimates [4] especially for the wrist and hand [5]. The technological methods available and used in studies have shown to produce reliable results [6], however, often at the expense of restraining the movement of subjects. This is due to bulky and wired-based sensor systems [7] [8] that anchor or constrict subjects to a limited amount of motions during measurements, as seen in figure 1.1. Furthermore, the methods are often complicated to use, which limits the use of technological measurement methods to mostly research purposes. Commercially available wearable sensors including electromyography (EMG) and wireless Inertial Measurement Units (IMU:s) could simplify technical measurements for ergonomists and reduce motion restriction.

Studies have demonstrated wrist angle, angular velocities and muscular load in the forearm as useful parameters when investigating wrist-related WRMDs [9]. Action limits for increased risk of wrist-related WRMD:s has recently been suggested in a report from Occupational and Environmental Medicine (Lund), based on angular velocity and muscular load. Velocities of 20°/s maintained 50% of a working day have been suggested as a threshold for wrist movement. For muscular load, thresholds of 30%_{MVE} maintained 10% of a working day, 10%_{MVE} maintained 50% of a working day and < 0.05%_{MVE} maintained 5% of a working day have been proposed [10].

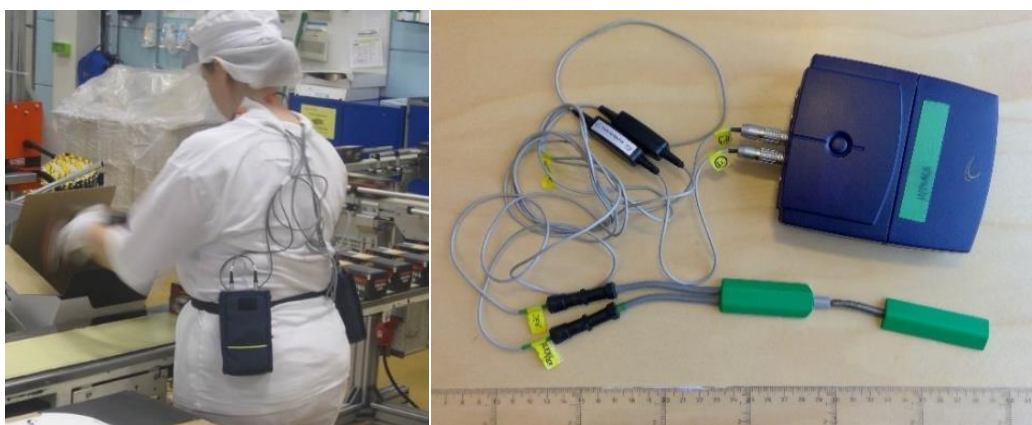


Figure 1.1: Measurement technology used in ergonomics.
Right: Electro goniometer and datalogger currently used by KI IMM
Left: Logger setup used with EMG on a subject during earlier research [11] (left).

1.2. Purpose and Goals

This thesis was a part of the project FORTE [12] at KI IMM (Karolinska Institute, Institute of Environmental Medicine) and consisted of developing a portable and simplified prototype system for measuring wrist activity and forearm load.

The main building blocks of the prototype would be comprised of:

- Acquiring Inertial Measurement Unit (IMU) sensor data on an Android device
- Acquiring Electromyography (EMG) sensor data on an Android device
- Processing sensor data to produce angles, angular velocities and muscular load
- Analyzing and visualizing information intuitively for exposure measurements in a web application.

2. Materials and Method

Hardware and software used during the development as well as tests performed are described in chapters 2.1 - 2.3. Table 2.1 presents a summary of the development and associated testing. All data processing outside of the applications were performed using Matlab 2018a (The MathWorks, Inc., Natick, United States).

Table 2.1: Development overview

Part/test	Purpose	Result
IMU		
2.1.2 Motion Generated Drift	Assessment of angle drift generated from biased motions w/wo. magnetometer correction	3.1.1
2.1.3 Magnetic Field Environment Test	Assessment of angle drift from indoor movement w/wo magnetometer correction	3.1.2
2.1.4 Static Angles Test	Determination of angular accuracies during static conditions	3.1.3
2.1.5 Dynamic Angles Test	Determination of angular accuracies during dynamic conditions	3.1.4
EMG		
2.2.2 EMG Signal Processing	Evaluation of different signal processing approaches	3.2.1
2.2.3 EMG Amplitude Test	Evaluation of EMG signals and physical contractions	3.2.2
2.2.4 Re-alignment Algorithm	Implementation of re-alignment algorithm using system sensors	3.2.3
Visualization		
2.3.1 Android application	Android Application	3.3.1
2.3.3 Data Visualization	Visualizing sensor data through web- and mobile-application	3.3.2

2.1. IMU

2.1.1. System Description

IMU:s of the model LPMS-B2 (LP research, Tokyo, Japan) were used for the development, see Appendix B for additional sensor specifications. Sensors data was sampled at 400 Hz and then resampled to 25 Hz [13] before being transmitted wirelessly (Bluetooth 2.1). To avoid the problem of gimbal-lock (Appendix A, 1.5), orientations were calculated in quaternions [14] provided by an extended Kalman Filter in the IMU firmware [15] [16].

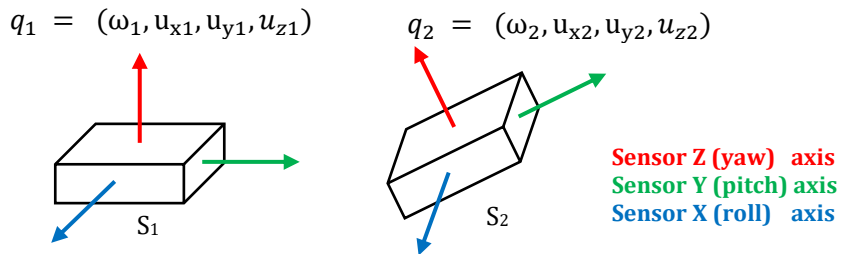


Figure 2.1: Rotations as quaternions.

The orientation of the two frames S1 and S2 can be described by their rotation-quaternions q1 and q2

Bluetooth transmitted IMU data was collected using an existing Android application developed at KI IMM and KTH [17] with modifications made using Android Studio v.3.1.0. Sensor rotations represented in figure 2.1 were derived from orientational data sampled from two separate IMU:s using equation 1.

$$q_{\Delta} = q_1^* \otimes q_2 \quad (\text{equation 1})$$

Equation 1: Calculation of the relative quaternion q_{Δ} from two quaternions q_1, q_2 .

The system clock on the smartphone running the application was used as a global timeframe. A joint timestamp between the sensors was calculated using equation 2, by pairing Android generated arrival-times from the individual sensors. Paired samples were determined by associating the latest timestamp from one sensor, t_{i1} , with the most recent timestamp from the remaining sensor, t_{i2} . Relative rotations were then derived from the associated quaternions of the timestamps, see equation 2.

$$t_{pair} = \frac{(t_{i2} - t_{i1})}{2} \quad (\text{equation 2})$$

Equation 2: Calculation of the joint timestamp between two paired samples.
 t_{i2} is the later sampled timestamp and t_{i1} is the earlier sampled timestamp.

2.1.2. Motion Drift

Studies have demonstrated the appearance of angular drift with the use of gyroscopes [18]. To quantify the problem, a test was constructed where two IMUs were configured to measure rotations with and without magnetometers included in their Kalman filters. They were fixed and aligned along a rotatable protractor with equal distance from the surfaces center. The setup was performed in an environment with low magnetic interference, this was measured using the magnetometers in the IMU:s. From this setup two different tests were performed, exposing the IMU to either biased (clockwise) or unbiased (clockwise and counter-clockwise) rotations. The gyroscopes and magnetometers were calibrated prior to both tests.

In the test with biased rotations, the protractor was rotated 5° clockwise in rapid successions every second until a total relative angle of 90° was reached. The IMU was then rotated back to the zero position in a significantly lower velocity to minimize the occurrence of motional drift. This motion was repeated 20 times. The test with unbiased rotations was performed using the same protocol, but with the previous rotations also performed counter-clockwise after returning to the starting position. Both test were performed 5 times and their respective results are presented in 3.1.1 (fig 3.1).

2.1.3. Magnetic Field Environment Test

The effect of movement in a large volume of space was also investigated. Two IMUs were attached to a ruler and aligned by their pitch-axis, simulating a “rigid” hand without any movement in the wrist (see fig. 2.2). Both orientation and magnetometers in each IMU was calibrated in the initial position. The ruler with the sensors attached was carried inside an office space in a predefined track (about 200 meters) with 10-sec pauses at predetermined stationary positions (4 horizontal, 1 vertical, see Appendix D5). This session was repeated 5 times without any additional calibration during the session. Result 3.1.2 (fig. 3.2 and 3.3) show the results from this test.

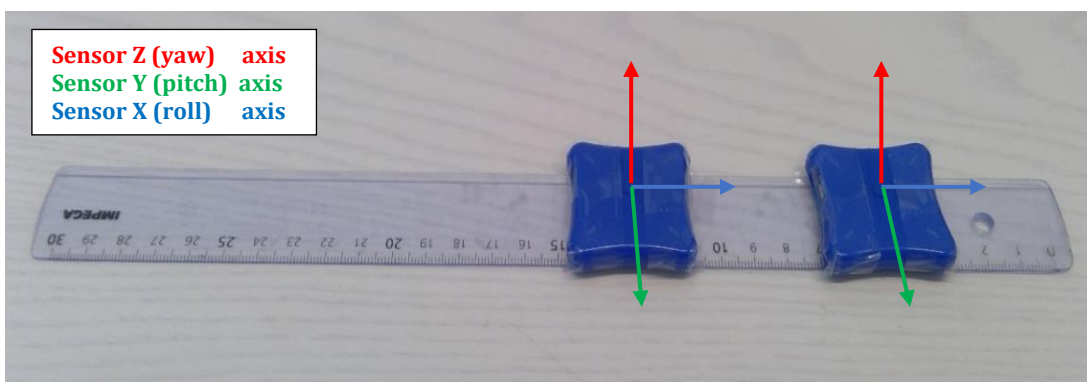


Figure 2.2: Magnetic field environment test setup.
Setup used for the field environmental test. Sensor axes indicated with red, green and blue.

2.1.4. Static Angles Test

For testing of the IMU's accuracy, a biaxial flexible goniometer (model *SG75*, Biometrics Ltd. UK, England [19]) and a datalogger (model *Mobi8*, TMSI B.V. Oldenzaal, NL) was used (see fig. 1.1). The two bodies of the goniometer were stacked and attached on top of each respective IMU. One IMU was then attached to a fixed horizontal plane while the other one was attached to the adjustable surface of a digital protractor (model *GAM 220 MF*, Bosch GmbH, Stuttgart, DE), with an accuracy of 0.1°. The protractor was rotated to 20 random angles in the vertical plane (range 0:90°) followed by rotations in the horizontal plane (range -30:30°). See result 3.1.3 (fig. 3.4, fig. 3.5) for Bland-Altman plots comparing pitch and yaw estimates from the goniometer and the IMU.

2.1.5. Dynamic Angle Test

Additional testing was performed to assess the performance of the IMU:s during dynamic conditions. Two IMU:s were placed over the third metacarpal bone of the hand (distally) and along the forearm (proximally) respectively, with the two bodies of the goniometer attached on top of the IMU:s, see figure 2.3. The zero-angle for both sensors was taken from a reference position with the subject resting the forearm on the table with 90° elbow flexion, as used in [20].

The subject performed near-maximum wrist- flexion/extension synchronized to a metronome signal (30, 60, 120 & 180 BPM) while keeping the forearm stationary. Each pace was performed for approximately 15 seconds. The signals were lowpass-filtered with a 31-point FIR filter (see appendix D4) with cutoff frequency 5.0 Hz [13], aligned in time and digitally resampled to 100 Hz to calculate the sample-to-sample error. Absolute angular velocities were calculated for both the goniometer and the IMU (both filtered with the FIR-filter described above) using a 3-point discrete difference $v_i = (\text{angle}_{i+1} - \text{angle}_{i-1}) / (T_{i+1} - T_{i-1})$ [13]. Root-mean-square-error (RMSE) was calculated (equation 3) for both angles and angular velocities. Two repetitions of the same test setup was performed. The second repetition included separate sampling and offline interpolation and alignment of the IMU signals using the sensors internal timestamps (not using equation 2), to evaluate the effect of synchronization errors. See result 3.1.4 (fig. 3.6 & tables 2.5-2.6) for data from the second repetition, and appendix B3-4 for additional data.

$$RMSE = \sqrt{\sum_{i=1}^n \frac{(Y_{\text{goniometer}}[i] - Y_{\text{IMU}}[i])^2}{n}} \quad (\text{equation 3})$$

Equation 3: RMSE, $Y[i]$ represent either angle or angle velocity for sample i .



Figure 2.3: Test-setup for simulated screw-sorting task.
Goniometer (green) stacked on top of IMU:s (blue)
The same sensor placement was used for all tests described in 2.1.5

A second test using the previous sensor setup was then constructed to simulate a practical working task of longer duration. The test consisted of manually sorting screws and bolts using one hand (see fig. 2.3). The first repetition lasted a total of 1h 16 min, the second repetition lasted 1h 2 min including five 2 min pauses. Result 3.1.4 (fig. 3.6 & 3.7) shows the distributions of velocities above/below 20°/s and velocity-bins of 5 °/s in the range 5–100°. Significance testing ($\alpha = 0.05$) of the velocity classification (20°/s) for the IMU and Goniometer was performed using a two-sided paired t-test, with the null hypothesis being no significance difference.

2.2. EMG

2.2.1. System Description

A wearable EMG-sensor (model *Shimmer3*, Shimmer Sensing, Dublin, IE) with configurable sampling frequency was used for measurement of the forearm muscle activity, see Appendix C for additional sensor specifications. Ag/AgCl-electrodes with dimensions 30x20 mm were used during all measurements. A Java/Android library provided by Shimmer [21] was used to modify the Android application implemented in 2.1.1, to interface both EMG and IMU:s over Bluetooth. See fig. 2.4 for EMG and IMU:s placement and size.

2.2.2. EMG Signal Processing

The common frequency for sampling surface EMG for ergonomic applications is 1024 Hz [22] [23]. The effect of using a lower sampling frequency of 512 Hz was experimentally investigated. A seated test subject performed 2 maximal reference contractions followed by 3 repetitions of 5 second static contractions (50 % max) and finally 3 repetitions of 5 second dynamic contractions (50 % max). Between each contraction, the subject rested for 1 minute. Surface EMG (see 2.2.3 for details) was sampled at 1024 Hz and then digitally resampled to 512 Hz. Two digital Butterworth filters were designed by convolving lower order filters to a combined 10th order filter [24]. See table 2.2 for filter specifications.

Table 2.2: EMG-filters and coefficients.
Filters and Matlab commands used to generate coefficients.

Filter	512 Hz filter	1024 Hz filter
Bandpass	<code>butter(2, [30/256 200/256]);</code>	<code>butter(2, [30/512 400/512]);</code>
50 Hz Notch	<code>butter(1, [49/256, 51/256], 'stop');</code>	<code>butter(1, [49/512 51/512], 'stop');</code>
100 Hz Notch	<code>butter(1, [99/256 101/256], 'stop');</code>	<code>butter(1, [99/512 101/512], 'stop');</code>
150 Hz Notch	<code>butter(1, [149/256 151/256], 'stop');</code>	<code>butter(1, [149/512 151/512], 'stop');</code>

$$\text{rms-EMG (n) [mV]} = \frac{\sqrt{x_{n-T}^2 + x_{n-(T-1)}^2 + \dots + x_n^2}}{T} \quad (\text{equation 4})$$

Equation 4: rms-EMG in millivolt, with a moving-window of length T = 64 samples. X_n is the filtered EMG output.

$$\text{rms-EMG (n) [%MVE]} = \frac{\text{rms-EMG (n) [mV]}}{\max \{\text{rms-EMG [mV]}\}} \quad (\text{equation 5})$$

Equation 5: rms-EMG in percent of maximal voluntary electrical activation.

Both signals (588 sec total length) were filtered, and a 125 ms rms-EMG [9] was calculated (equation 4) and MVE-scaled (equation 5). The 1024 Hz data was filtered with the forward-backward filtering using the Matlab *filtfilt*-function [25]. Result 3.2.1 (fig. 3.9) shows the distribution of samples using the two signal processing approaches. The 512 Hz alternative was chosen and implemented as a real-time filter and moving-window processing (equation 4 & 5) in the Android application.

2.2.3. EMG Amplitude Test

Two IMU:s were attached to the arm and hand as described previously (see 2.1.5). A pair of EMG electrodes were then attached to the muscle belly of *m. extensor carpi radialis*, approximately one third of the forearm length down the elbow and with an electrode center-to-center spacing of 2 cm [26] [22]. A reference electrode was placed over the *olecranon* [27]. Skin was prepared with sandpaper and disinfectant (alcohol) at the electrode site.



Figure 2.4: EMG and IMU:s.
A: EMG-electrode and IMU placement for test.
B: Top: EMG-circuit (Shimmer Sensing, Ireland), bottom: IMU:s (LP Research, Japan).

The test started with the subject resting the forearm measured on an armrest with approximately 90° elbow flexion. Three maximum contractions were performed using a hand dynamometer (Baseline, Irvington NY, US). This was followed by 4 submaximal 5 second static contractions (50% max) and 4 submaximal contractions (50% max) combined with wrist flexion/extension performed during 5 seconds at 40 bpm. Flexion/extension was also performed in the same manner without any load. Each session (4 static contractions 4 dynamic contractions and 4 zero-load flexions/extension) was performed with 30 - 60 second rest in between. A total of 4 sessions were performed with, 1-minute rest in between. See 3.2.2 for the EMG signal and amplitude analysis from the test (fig. 3.10-3.12).

2.2.4. Re-alignment Algorithm

Earlier results (see 3.1.1 and 3.1.2) indicated that the relative angle in the horizontal plane is subjected to a significant drift during movement in a large volume and/or from biased rotations. To this end a *re-alignment* algorithm was developed and implemented in the android device. The algorithm was based on the idea of correcting the angular drift between the two sensors by combining sensor data from both IMU:s and EMG. Through the combined data, assumptions were made regarding the position of the joint in certain situations.

Table 2.3: Parameters in re-alignment algorithm.

Parameter	Unit	Description
$\mathbf{q}_1, \mathbf{q}_2$	[quaternion]	Orientation output from sensor 1 and sensor 2
\mathbf{q}_{corr}	[quaternion]	"Error-rotation" between the two systems
$\mathbf{q}_{1,C}$	[quaternion]	Re-aligned output from sensor 1
\mathbf{q}_Δ	[quaternion]	Relative angle after correction
Gyr_1	[deg/s]	Gyroscope component around sensor 1 yaw-axis
Acc_2	[m/s ²]	Accelerometer component along sensor 2 (negative) yaw-axis
rms-EMG	[%MVE]	RMS output from the EMG measurements of the forearm extensors
T	[sec]	Length of time window

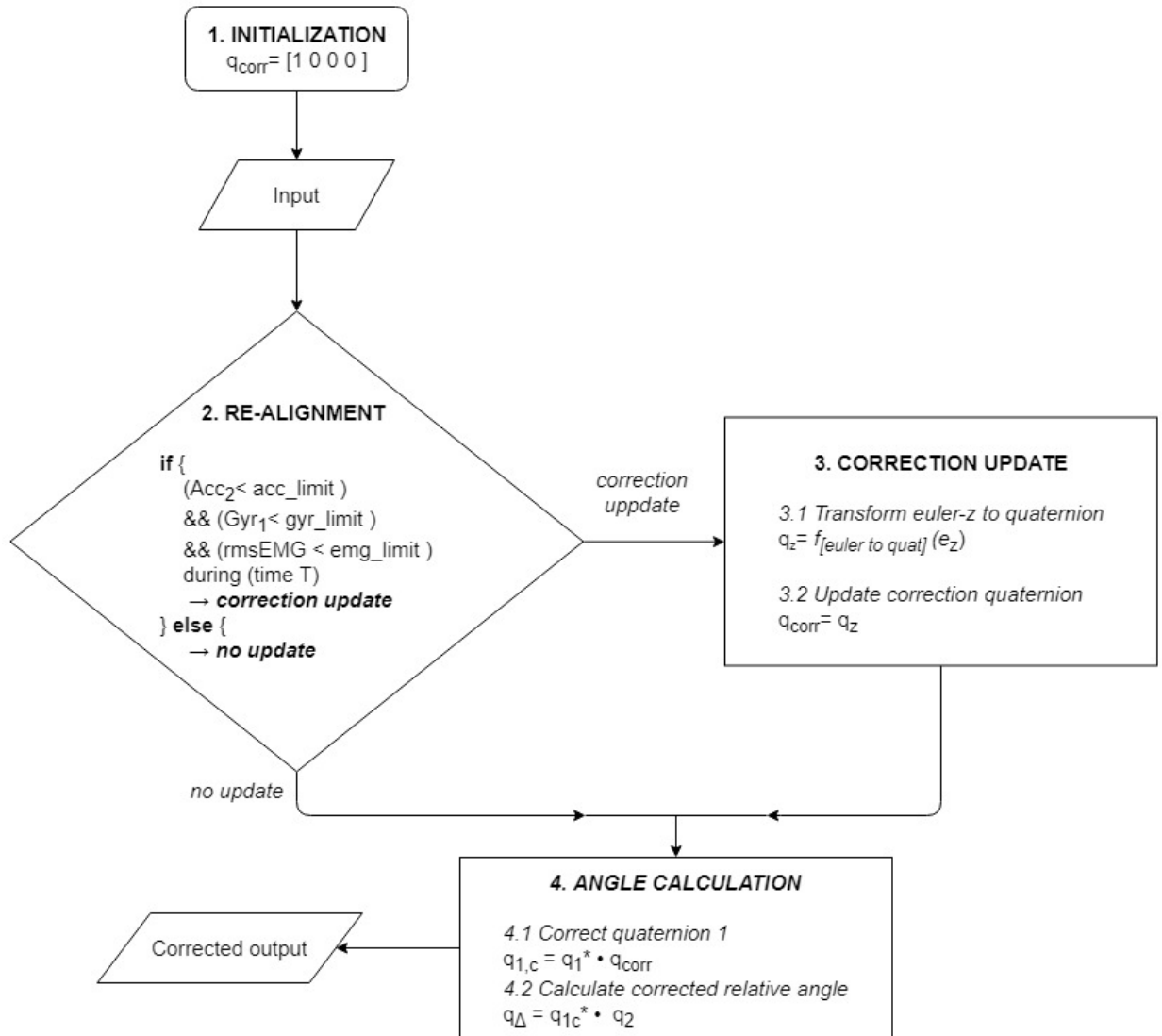


Figure 2.5: Flowchart of the re-alignment algorithm.
The four major steps are: (1) initializing the correction to zero, (2) checking the alignment-criteria,
(3) updating the correction and (4) calculating the corrected output.

The algorithm aims to detect periods when the forearm is in a horizontal resting position and assumes that an ulnar/radial angle is typically in a neutral (0°) position during this time. The accelerometer-, gyroscope- and rms-EMG signal are not subjected to drift on a short time-scale (as opposed to the relative angle) and are therefore used to correct the latter. If a resting period is detected the relative angle in the horizontal plane is assumed to be an error and used for correction of subsequent samples. Fig. 2.5 describes the algorithm, table 2.3 lists the algorithm parameters.

Table 2.4: Parameter-limits used for re-alignment test.

Parameter	Unit	Limit
Gyr ₁	[deg/s]	[2, -2]
Acc ₂	[m/s ²]	[-1.25, -0.75]
rms-EMG	[%MVE]	< 2
T	[sec]	1.7

A test was conducted to evaluate the realignment-algorithm. Table 2.4 lists parameter-limits used. Two mock-up “work-tasks” were constructed: the first being rapid flipping through a notebook (task 1). The second task consisted of connecting dots arranged horizontally on a computer screen at a fixed pace (30 BPM) using a mouse with a stationary forearm (task 2). Four repetitions were performed, each including task 1 and task 2 performed in a sequence. The test-subject rested the forearm horizontally for 5 seconds when switching between tasks. Figure 2.6 shows the resting position between the tasks with sensor placement (A) and the test-person view during task 2 (B). See result 3.2.3 (fig. 3.13) for the result of the test.

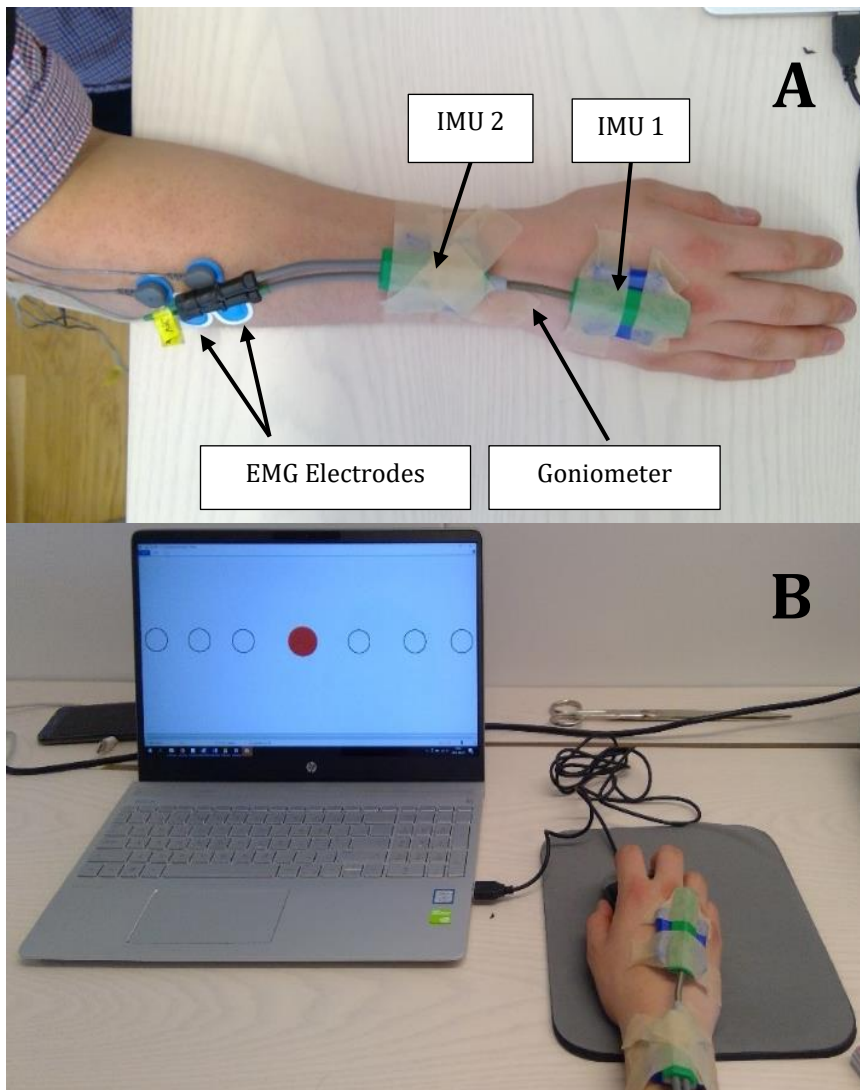


Figure 2.6: Re-alignment algorithm test setup.

A: Resting position with location of EMG-electrodes, goniometer and IMUs.

B: Test person view during task 2.

2.3. Data storage and visualization

Data from sensorsFor online storage and visualization of the sensor data a cloud-database was used, and a web-application was developed.

2.3.1. Database and Data Modelling

The data sampled by the Android application was transferred as 15-second-long JSON-data packages using the MQTT-protocol. The Eclipse Paho Android Service library¹ and a public message broker provided by HiveMQ² was used. The sensor data was stored using the open-source document-database MongoDB provided online as a database as a service³. To avoid overreaching the MongoDB document-size limit [28] and balancing the tradeoffs of updating vs inserting new documents [29] [30], 1-minute nested-documents was used. A data-model combining referencing and embedding was implemented. One collection (*measurements*) holds documents with information related to a single measurement (id, date, duration) and the number of associated data documents. Documents in the *data*-collection holds the sensor data (angles, EMG, timestamps) stored under separate document fields. See fig 2.8.

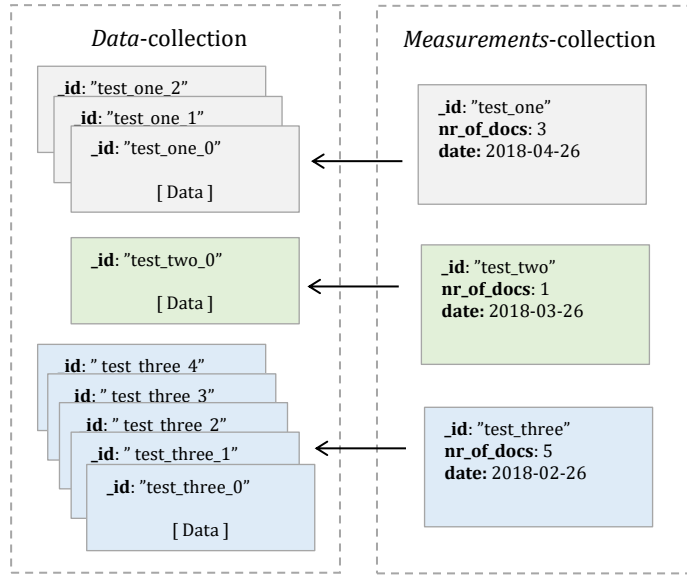


Figure 2.7: Modeling sensor data in MongoDB
Each document in the measurements collection is associated to a set of data documents.

2.3.2. Data Visualization

A web-application was developed using the flow-based development tool Node-RED and deployed to IBM:s cloud platform *Bluemix*. The application acts as an interface to the database, both implementing the data model and allowing a user to load and visualize a measurement through a web-browser (see fig. 3.15). The main structure of the program is built using JavaScript, combined with a Node.js driver for MongoDB and UI-components based on angular.js (provided through the Node-RED environment). Measurements are queried from the database by searching for an id. An initial query is made to the *measurements*-collection. Given a match, the number of documents in the *data*-collection associated to the measurement is passed back to the application. A processing-sequence is then performed during which all *data*-documents for the id are queried, loaded into the application memory, processed and analyzed in series. Parallel to the web-based visualization, direct feedback of IMU and EMG data was implemented in the Android application (see fig. 3.14). This included feedback from EMG calibrations.

¹ <https://www.eclipse.org/paho/clients/android/>

² <https://www.hivemq.com/try-out/>

³ <https://www.mongodb.com/cloud/atlas>

3. Results

Results from testing and development are presented in chapters 3.1-3.3

3.1. IMU

3.1.1. Motion drift

Figure 2.1 shows the accumulated drift between each repetition. Biased motion is seen to generate larger amounts of drift.

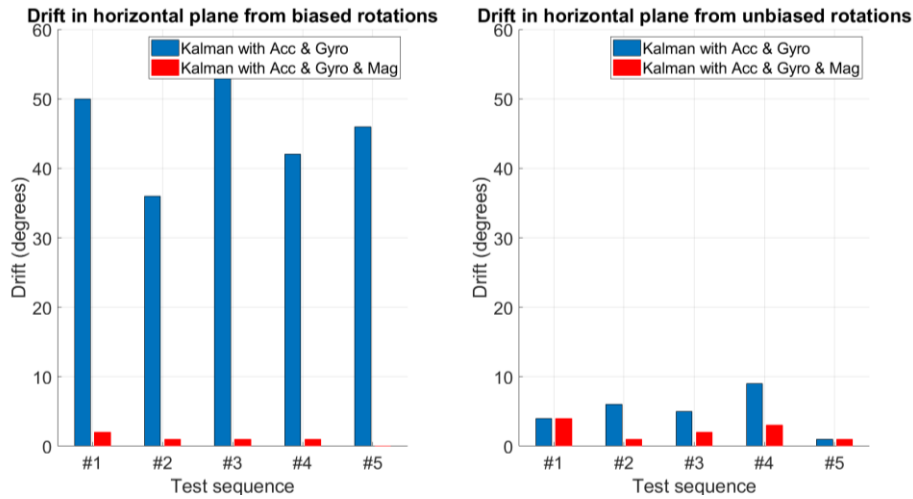


Figure 3.1: Motion generated drift.
Angular error from biased rotations (left) and unbiased rotations (right).

3.1.2. Magnetic Field Environment Test

The appearance of drift from the magnetic field environment tests in the three sensor axes (top) and the total error (bottom) can be seen in figures 3.2 and 3.3 respectively. Both IMU configurations (w/o magnetometer) generates substantial angle error.

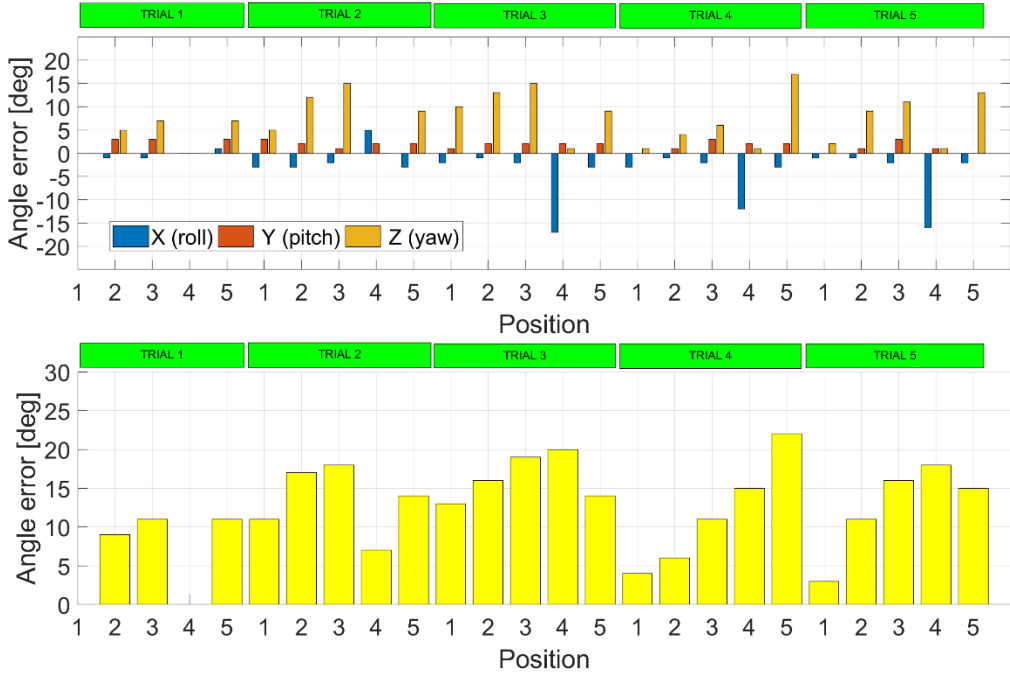


Figure 3.2: Environmental test, with magnetometer.

Error built up in individual 3-dimensional axes (top graph). Sum of total error for each position (bottom graph)

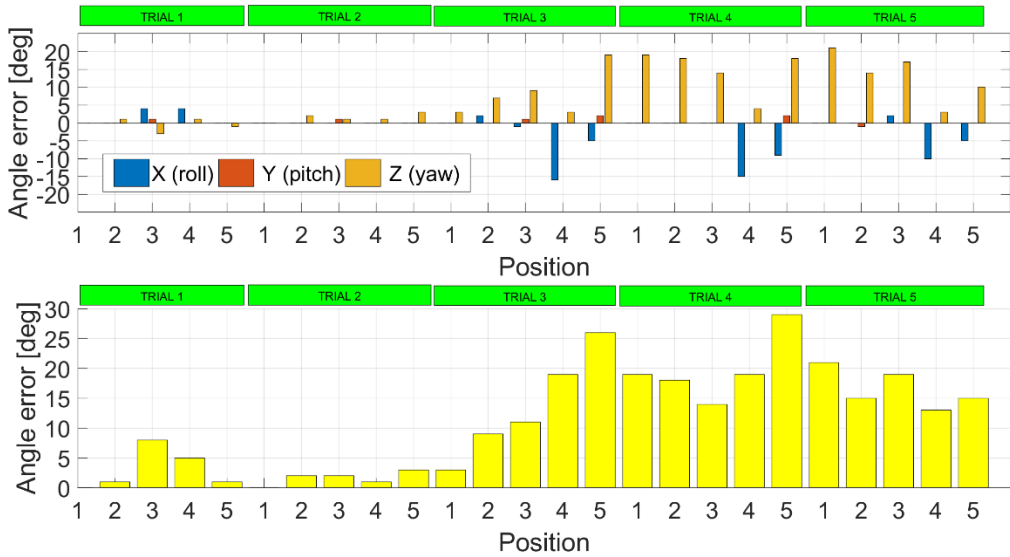


Figure 3.3 Environmental test, without magnetometer.

Error built up in individual 3-dimensional axes (top graph). Sum of total error for each position (bottom graph)

3.1.3. Static Angles Test

The comparison of goniometer and IMU performance from the static angle test are shown in figures 3.4 and 3.5 in the form of Bland-Altman plots. The pitch and yaw estimations from both systems are separately compared in respective figures. IMU:s measured pitch with higher accuracy than goniometers, however, for yaw goniometer showed higher accuracies.

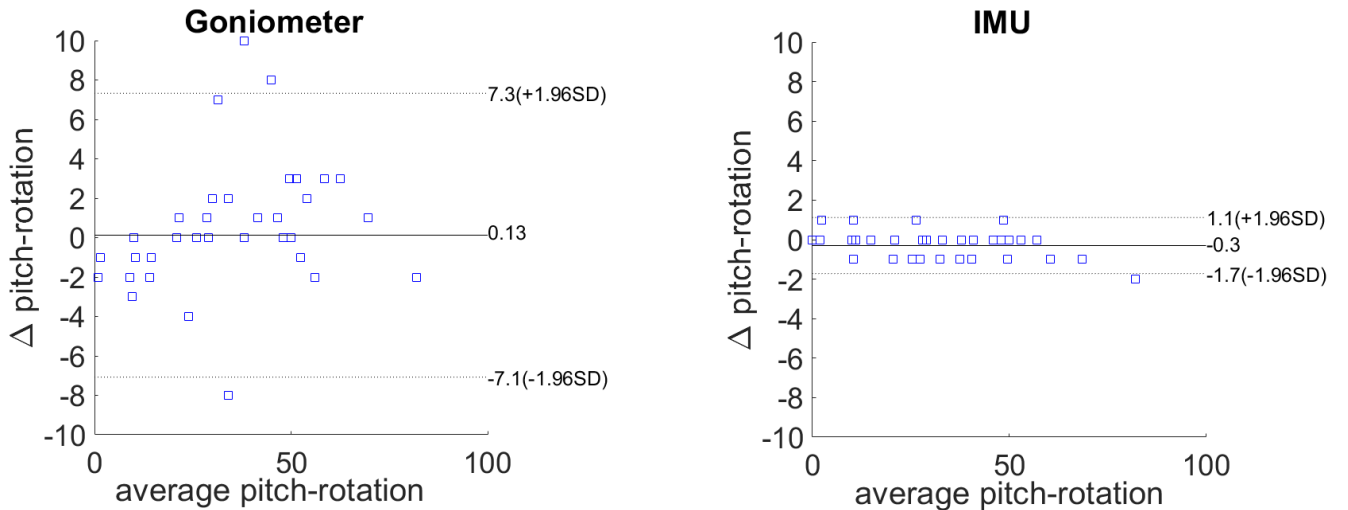


Figure 3.4: Bland-Altman plot, pitch rotation.
Static angle test (vertical plane) with pitch-rotations using Goniometer (left) and IMU (right).

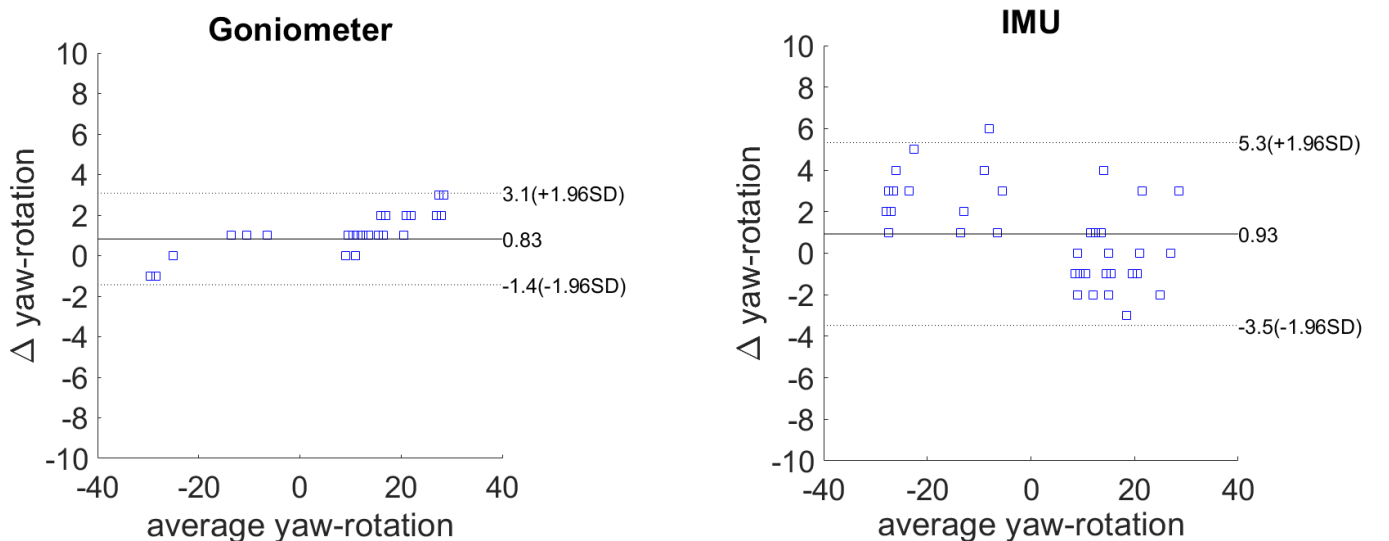


Figure 3.5. Bland-Altman plot, yaw rotation.
Static angle test (horizontal plane) with yaw-rotations using Goniometer (left) and IMU (right).

3.1.4. Dynamic Angles Test

Figure 3.6 shows the angular estimations of the IMU and goniometer from the 120 BPM part of the second repetition. RMSE for angles and angular velocities for the four paces are presented in tables 2.5 & 2.6. See Appendix D1 for remaining results of the first repetition and Appendix D2 for results from the second repetition. Drops in sampling frequency (fig. 3.6, bottom) coincide with periodic distortions in the angular signal (fig. 3.6, top). Table 2.5 and 2.6 show RMSE of angles and angular velocities.

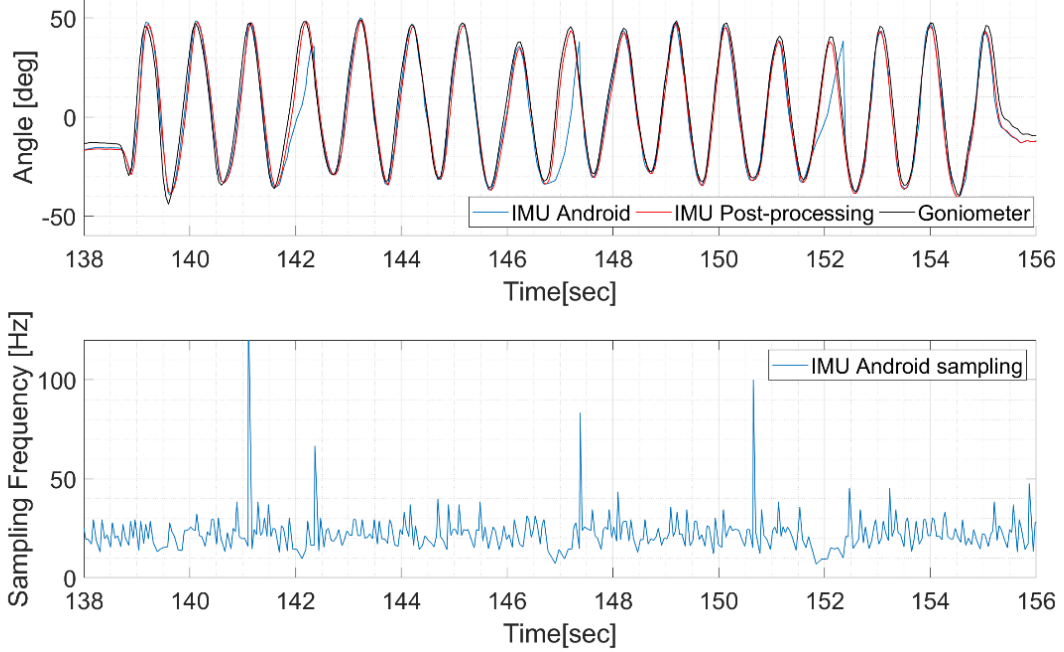


Figure 3.6: Wrist extension/flexion at 120 BPM.

TOP: IMU angle from Android app (blue), IMU from off-line processing (red) and goniometer (black).
BOTTOM: Periodic drops in the sampling rate of the IMU:s in the Android application (blue, bottom) distorts the IMU signal (blue, top).

Table 2.5: RMSE of angles from dynamic angle test.

Test sequence	RMSE (angles) [°]	
	Android	Offline processing
30 BPM	4	4
60 BPM	6	4
120 BPM	10	6
180 BPM	11	6

Table 2.6: RMSE of angular velocities from dynamic angle test.

Test sequence	RMSE (angular velocity) [°/sec]	
	Android	Offline processing
30 BPM	15	8
60 BPM	36	15
120 BPM	70	38
180 BPM	112	47

The results from the first and second repetition of the one-hour screw-sorting tasks are seen in figures 3.7 and 3.8 respectively. Absolute angular velocity's in $5^{\circ}/\text{sec}$ -bins in the interval $[5,100] ^{\circ}/\text{s}$ (left) and above/below $20^{\circ}/\text{s}$ (right) for both goniometer (red) and IMU (blue) are shown. Tables 2.7 and 2.8 presents the same velocities in percentiles, a format commonly used in ergonomic research [9].

Figures 3.7 and 3.8 (left) suggested that the IMU:s tended to underestimate velocities above $20^{\circ}/\text{s}$ and overestimate velocities below $20^{\circ}/\text{s}$. However, the 2.8% and 4.1% classification differences (fig. 3.7 and 3.8, right) were not found to be statistically significant.

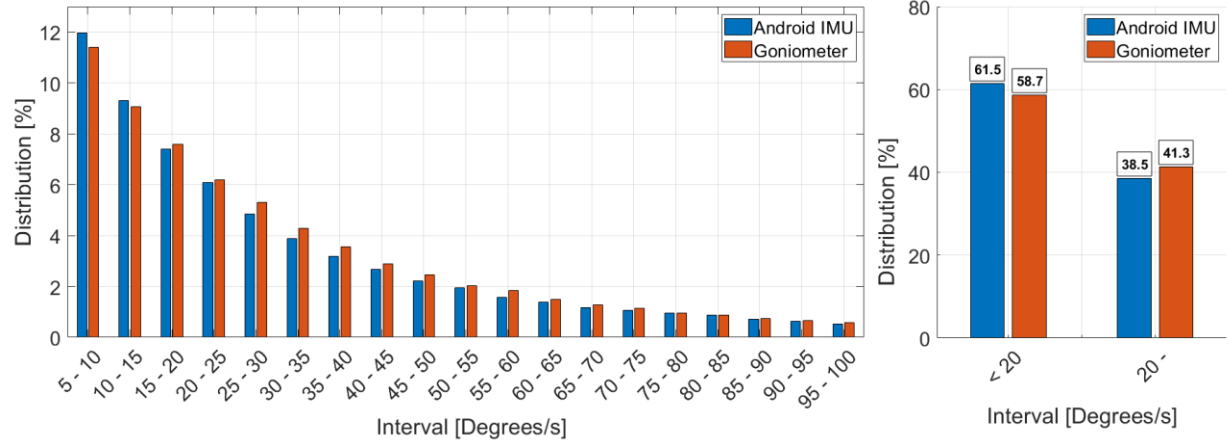


Figure 3.7: Angular velocity distribution (first repetition)

Velocities distributed in $5^{\circ}/\text{s}$ wide blocks(left). Velocities distributed in two blocks, below and above $20^{\circ}/\text{s}$ (right)

Table 2.7: Angular velocity in percentiles (first repetition).

Percentiles	angular velocity [$^{\circ}/\text{s}$]	
	IMU	Goniometer
10 th	0.6	0.6
50 th	10.0	12.8
90 th	50.0	53.8

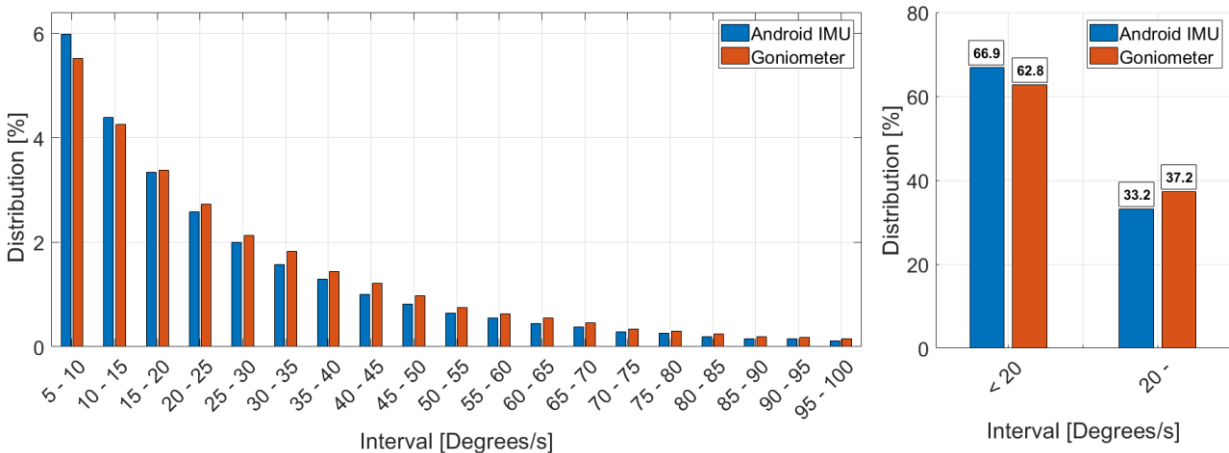


Figure 3.8: Angular velocity distribution (second repetition)

Velocities distributed in $5^{\circ}/\text{s}$ wide blocks(left). Velocities distributed in two blocks, below and above $20^{\circ}/\text{s}$ (right)

Table 2.8: Angular velocity in percentiles (second repetition).

Percentiles	angular velocity [°/s]	
	IMU	Goniometer
10 th	0.2	0.1
50 th	12.7	14.4
90 th	67.6	70.0

3.2. EMG

3.2.1. EMG Signal Processing

Figure 3.9 shows the distribution of the rms-EMG signal (588 sec total length) according to action limits (Lund). Signals sampled at 1024 Hz and 512 Hz are compared.

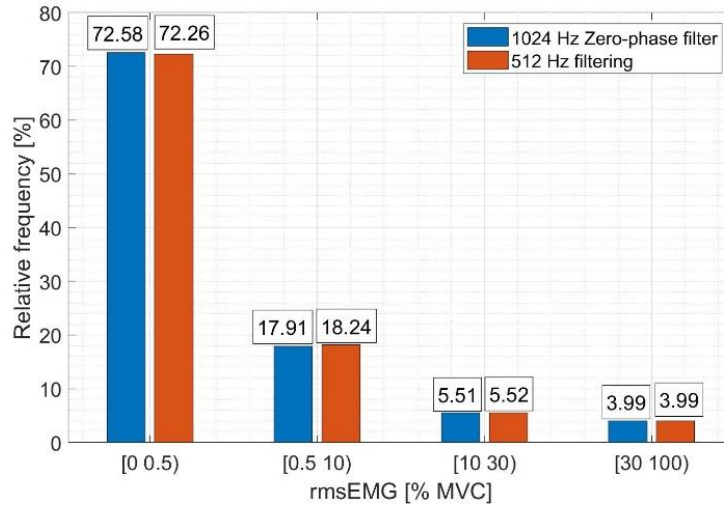


Figure 3.9. EMG signal-processing sample distributions.

Relative distribution of rms-EMG samples from the same measurements analyzed with 1024 Hz (blue) and 512 Hz (red) processing steps.

3.2.2. EMG Amplitude Test

Results from the EMG amplitude tests can be seen in figure 3.10 - 3.12. Figure 3.10 and 3.11 shows EMG amplitudes during static contractions (top), dynamic contractions (middle) and unloaded flexion/extension (bottom). Figure 3.12 demonstrates the appearance of muscular rest ($0.5 < \%MVC$, green blocks) together with wrist flexion/extension and rms-EMG.

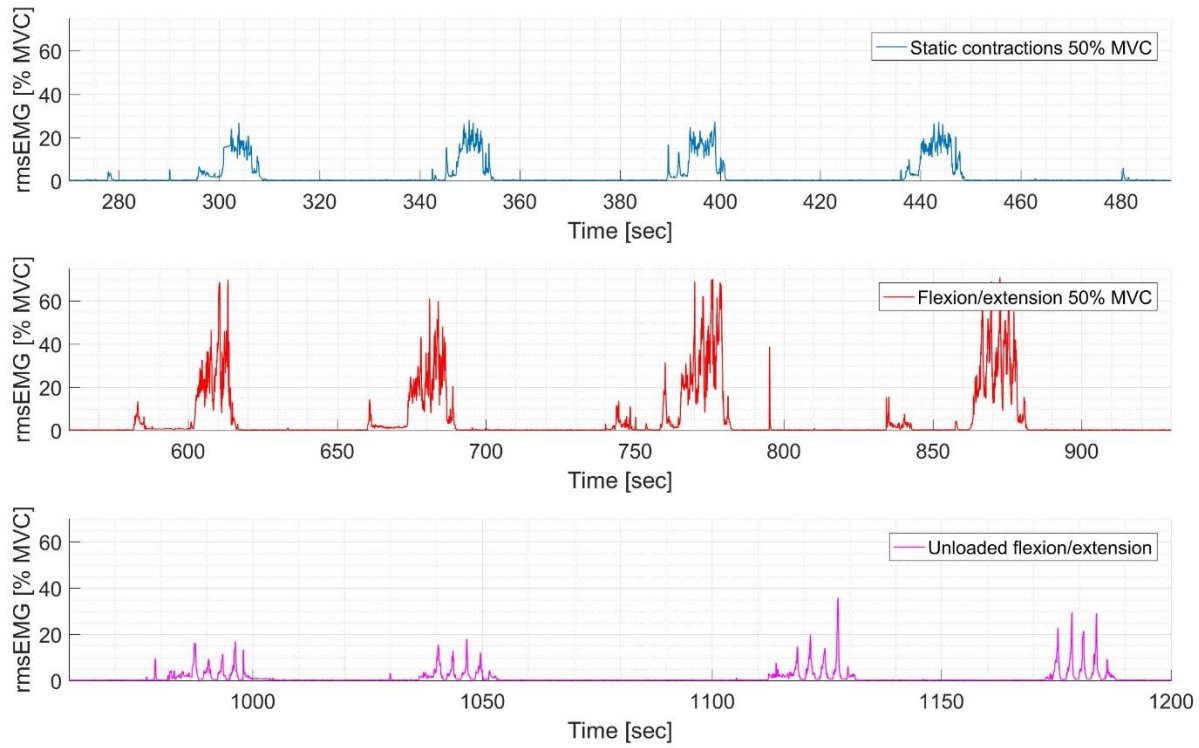


Figure 3.10: EMG-amplitudes from contraction test.

Static contractions (blue) extension/flexion during static load (red) and extension/flexion without load (purple).

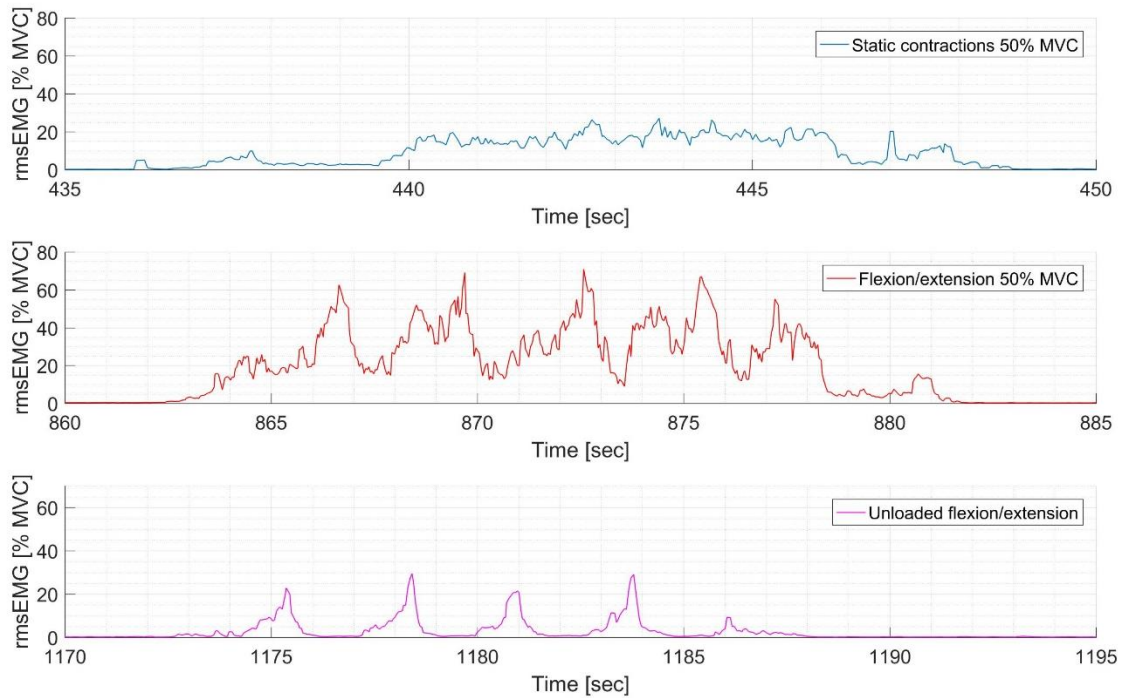


Figure 3.11: EMG-amplitudes from contraction test, last repetition seen in figure 3.10.

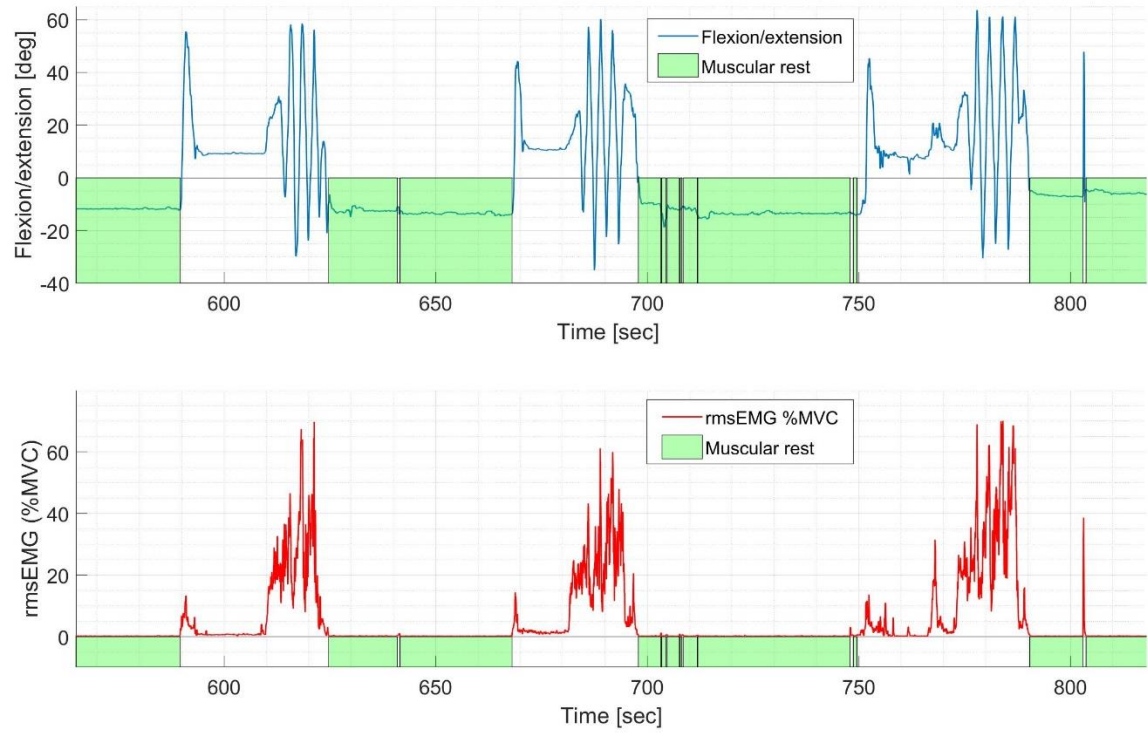


Figure 3.12: Wrist and muscular activity during loaded flexion/extension.
The first three loaded extension/flexions Bottom: Sections of minimum 300 ms continuous muscular rest (green, <0.5 %MVE) of rms-EMG (red) Top: The same rest-periods (green) with the angular signal from the IMUs (blue).

3.2.3. Re-alignment Algorithm

Figure 3.13 show the radial/ulnar angle during 4 sequential repetitions of task 2. A gradual build-up of angular drift occurs between each sequence in the uncorrected IMU angle (red) compared to the goniometer (yellow) reaching over 40° for the last sequence. This drift is eliminated using the re-alignment algorithm (blue).

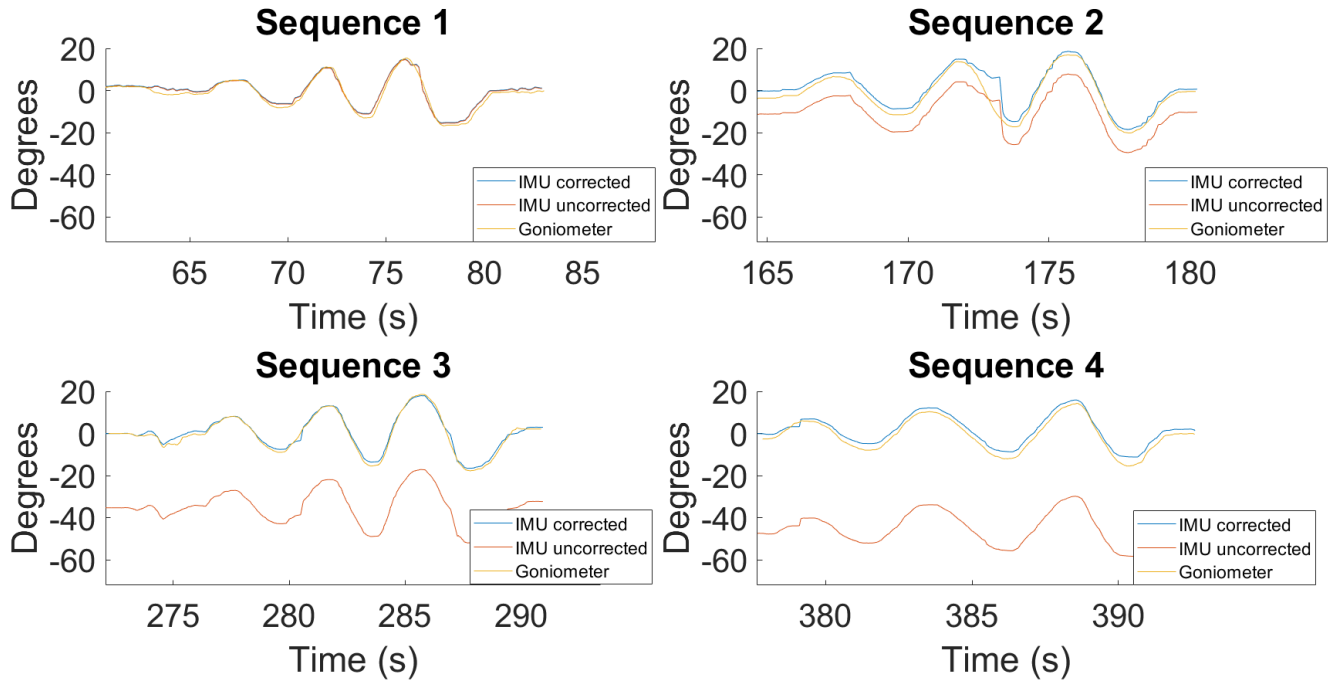


Figure 3.13. Re-alignment algorithm test.
Ulnar/radial deviation angle measured with the goniometer (yellow), IMU without corrective algorithm applied (red) and IMU with the correction algorithm (blue) for the first four repetitions of task 2.

3.3. Data storage and visualization

Real-time feedback is provided in the Android application during a measurement (3.3.1), and whole measurements are processed and visualized in the web-application (3.3.2).

3.3.1. Android application

Real-time feedback of the IMU and EMG data was provided on the Android application as presented in figure 3.14. Additional functions in the application included a offset function for the relative angle and and a controlled reference measurement for MVE normalization of the EMG signal. The automatic re-alignmet algortihm described in 2.2.4 and 3.2.3 runs in real-time in the application.

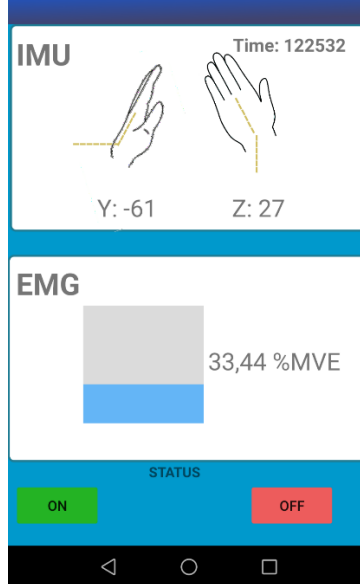


Figure 3.14. Interface for the Android application.
Top: Flexion/extension and deviation angles. Bottom: Forearm rms-EMG amplitude

3.3.2. Web application

Figure 3.15 shows measurements from part 2.1.5 viewed through the web-application using a web browser. Distribution of angular velocity for wrist flexion/extension (top middle) and rms-EMG (lower middle) and action-limits suggested by Lund, as well time-averaged signals (right) are presented. Measurements are loaded from the database using a search function (top left). Note the increased time in muscular rest (0 vs 5 %) as well as decreased time at high angular velocitys (41 vs 48 %) for the task with scheduled pauses (B) as oppose to the one without any rest (A).

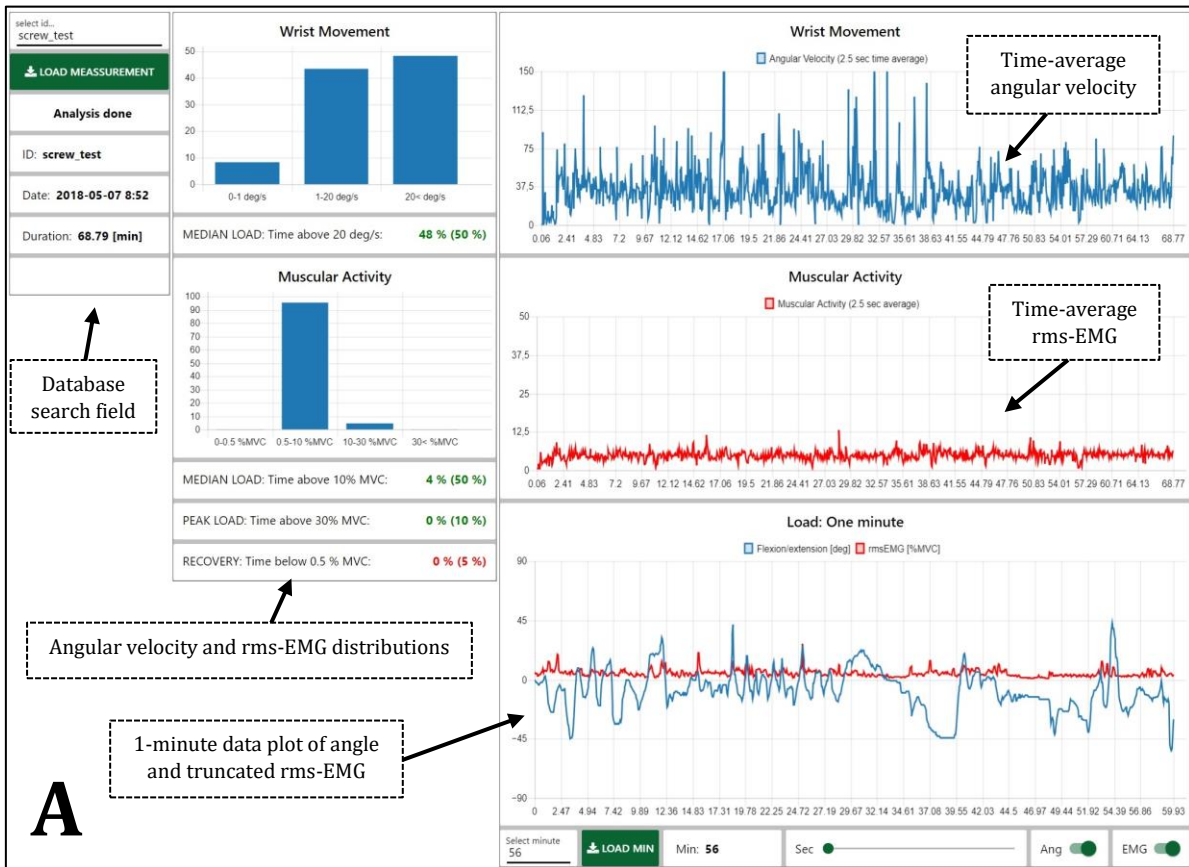


Figure 3.15: Interface for the web application.

A: 1 hour and 8 minutes of continuous work, without any rest. Minute 56 loaded in detail view.
B: 1 hour of the same task with periodic rests, giving an increased muscle recovery time (15 vs 0 %).

4. Discussion

Result 3.1.1 indicated that the difference in angular drift from both biased and unbiased rotations remained small when using magnetometer correction (fig. 3.1 right). Not using the magnetometer correction (fig. 3.1 left) caused larger error during biased movement. This was expected as relying solely on the integrated gyroscope signal exposed the measurements to integration errors [31]. Smaller error for unbiased movements also agreed with findings by [32] where unilateral rotations was found to give larger errors than multi-axis rotations (albeit with different sensors and protocol at higher velocities). It is likely that the error is proportional to both direction of movement and velocity, and that evenly distributed movements of opposite direction partly reduces this error. The magnetometers were calibrated in the stationary position before the start of the test. This likely improved its performance (see 3.1.2).

Part 2.1.3 investigated the effect of movement in a large indoor volume. The total angle error grew large both with (max 22°, fig. 3.2 bottom) and without (max 29°, fig. 3.3 bottom) the magnetometer. The error was typically confined to the horizontal axes (fig 3.2 & 3.3 top) which agrees with previous methods using differential measurements with a pair of IMU:s [33]. The rapid build-up of error when using the magnetometer compared to relying solely on the gyroscope could be an effect of the changing magnetic field when moving between two positions. IMU angular errors from inhomogeneous indoor magnetic fields have been reported to be 16° (indoor track with test objects) and 29° (movement in a motion lab) [34], reaching up to 35° in the vicinity of metallic objects [35]. This seems to be within range of what we found, however differences in test-protocol, sensor model and duration makes exact comparison difficult. This result indicates that magnetometer is of limited use for indoor measurements, and that an error in the relative angle will build up over time regardless of its use. However, only a single indoor environment was investigated, also because we were limited to one sensor model (and decided to use the sensor fusion algorithm embedded on the device) the effect of other IMU models and/or alternative sensor-fusion and magnetic compensation algorithms was not investigated. The IMU's sensitivity to both biased movements (which could occur during e.g. hammering) and error build-up from indoor movement (even at "normal" environments, see Appendix D5) was used as the rationale for developing the re-alignment algorithm described in 2.2.4.

In 3.1.3. the pitch estimation from the IMUs in stationary angles demonstrated a 1.96 standard deviation from -1.7 to 1.1°. The estimation of the corresponding goniometer, however, exhibited a range from -7.1 to 7.3°. The smaller uncertainty of the IMU may indicate that when properly corrected by accelerometers, the sensor tracks stationary angles with satisfying accuracies. Similar results are also presented in studies, demonstrating accuracies of accelerometers and gyroscopes to below 3° [6] [36]. Without any sensor correction, the yaw estimation of the IMU demonstrated instead a 1.96 standard deviation range from -3.5 to 5.3 °. Compared to the goniometers range of -1.4 to 3.1°. The test confirmed prior established characteristics of the gyroscopes in 3.1.1, however, the drift exhibited in the horizontal axis may accumulate indefinitely with continuous biased rotations in the horizontal axis.

While we used goniometry as a reference method, it is not the golden standard of the field [8], due to "cross-talk" and zero-drift [37]. Goniometers have been shown to measure angles with mean uncertainties of 8° in flexion/extension and up to 21° in deviation [8] [37]. These errors can be reduced to < 1° with compensating methods, using for example torsiometers [38]. However, large scale studies have used goniometers for establishing risk-exposure relationships without these modifications [6]. This suggests that errors from IMU:s (under static conditions) may lie within the limits of acceptance.

Results 3.1.4 showed that RMSE of the IMU angles ranged from 4° (30 BPM) to 11° for (180 BPM). The corresponding RMSE for angular velocity ranged from 15°/s to 120°/s. A second repetition of the same protocol (Appendix D1, table D1.1), similarly showed errors proportional to velocity,

with an RMSE for angles of 8° (30 BPM) to 21° (180 BPM) and corresponding velocity errors from 29°/s to 180 °/s. The angular errors were comparable to previous findings of the same model of IMU [17]. Using an Optical Motion Capturing (a golden standard), angle RMSE was found to be between 3.6° to 7.5°. The smaller errors in this study are likely a result of our method for sensor pairing (see below), IMU and goniometer signal misalignment [39], but possibly also due to the higher velocities, alternative reference methods and movements (wrist- flexion/extension \geq 30 BPM vs. trunk flexion/extension at 20 BPM).

Manual inspection of the signals (figure 3.6) indicated that errors may have been a result of reoccurring signal distortions related to irregular IMU sampling. Bluetooth communication has demonstrated restrictions such as delay and packages loss [40] [41], a phenomenon detected in the IMU:s used in the thesis (figure D3, Appendix D). The timestamp paring (equation 2) did not consider these factors and instead used the arrival times of Bluetooth packages as timestamps. Independent sampling and offline-synchronization (using the sensors generated timestamps) gave increased accuracy for both angles (table 2.5) and angular velocities (table 2.6). This indicated that the combination of Bluetooth issues and choice of synchronization contributed to the error. Alternative offline timestamp identification and pairing such as the ones used in MATLAB should be investigated, as well as methods for real-time sensor time synchronization in the Android application, which have been described in the literature [41] [42].

In the work-task test, both repetitions were presented in absolute distributions and percentiles, to resemble formats used in exposure studies [9]. The IMU and goniometer differences (2.8% & 4.1%) in velocity classifications at 20°/s were not found to be statistically significant. However, this was based on only two repetitions, making the statistical power questionable and the risk of type-II errors non-negligible [43]. Furthermore, both repetitions were performed under semi-controlled conditions under limited time-periods. This limits any certain conclusions to be drawn regarding the classification accuracy. Additionally, velocity estimations will be affected by the inaccuracies shown in the dynamic accuracy testing (3.1.4) even though this test featured angular velocities mainly above the 20°/s cut-off limit. Furthermore, accuracy under long-term measurements (and situations with biased motions) could be dependent on successfully handling the relative angle error (as discussed in 2.2.4). For long term measurements, a solution to the accumulating errors may be to derive angular velocity directly from the gyroscopes.

Result 3.2.1 (fig. 3.9) indicated that the effect of the alternative 512 Hz sampling and processing of the EMG was small when classified according to suggested amplitude categories (Lund). This result agrees with earlier findings that lowering the sampling rate to 512 Hz has little impact on amplitude analysis of smoothed EMG waveforms [44], however this study used a 5-ms moving average filter as opposed to our 125ms-RMS. Also, our measurement was limited to ten minutes and only included a few contractions/movements, longer tests should be performed to further investigate this effect. This approach has the benefit of enabling real-time processing and presentation of the rms-EMG in the Android application (useful as feedback during e.g. a calibration procedure), and also reduces the volume of the data. The downside is the increased battery drain and possibly performance issues when running on different hardware⁴ [45].

The concept of an automatic re-alignment method to compensate for poor horizontal IMU estimation has been described in literature for both elbow [46] and knee joints [18] [47] [48]. While this problem could also be addressed by investigating alternative algorithms for handling magnetic field disturbances, these typically require detailed knowledge of the sensors, filters and are complicated to implement [49] [50]. More so, focusing on optimizing individual sensor performance when a pair of IMU:s are used for differential angle measurement is probably futile, due to the unavoidable inter-sensor differences (including experienced inputs and fabrication effects). Anticipating, detecting and adjusting the error provides a more general solution. Results

⁴ Application tested on Huawei Honor8, Samsung Galaxy Tab A & Samsung Galaxy A3 2017

presented in 3.2.3 demonstrated one implementation of a generic re-realignment algorithm, using both IMU and EMG data. The test was however limited, using artificial tasks and controlled rests. Further tests on blinded subjects are required to determine additional resting-postures and to generate more strict realignment parameters.

Regarding the database, the presented data-model (fig. 2.7) has benefits in terms of performance (avoiding frequent inserts and reads/updates of large documents) and has been suggested for storing sensor data in MongoDB [29]. Furthermore, it naturally supports rapid querying and block-processing of the data during readout (required by the limited free-trial runtime memory in the web application). However, it is also complicated to implement in the case of non-uniformly sampled signals where accurate document-splitting must consider a varying sample-rate, potentially making querying specific time periods from long measurements difficult. Other noSQL databases without the 16 MB BSON document size limitation [51] or traditional SQL-databases with more flexible queries [52] could also be investigated.

The web-application presents the forearm load both in terms of time-trend signals as well as amplitude distributions and calculated action limits. Regarding the EMG, result 3.2.2 (fig. 3.12) suggest that rms-EMG can be classified according to the Lund action-limit for rest, and in 3.3.1 we show how this can be used in the web-application for visualizing 1h measurements (3.15 A), and the effect of periodic pauses (fig 3.15 B) on the muscular load classification. However, these results were obtained under controlled conditions of limited duration using simulated tasks. Factors including successful reference contractions, electrode placement [53], movement artefacts [54] and environmental noise [55] encountered during real-life ambulatory field-measurements will affect the measurements to a great extent. This could require additional processing and filtering steps to be implemented prior to amplitude classification. Also, specific physiological phenomena like increased EMG amplitudes seen during fatigue makes the very concept of EMG-amplitude as a measure of muscle activation non-trivial [56]. For the angular velocity, because of the inaccuracy of the velocity classification (result 3.1.4) the presented distributions and action-limits are not accurate, even though the trend is correct and periods of high/low wrist movement can be grasped in a qualitative sense (fig. 3.15 A&B). Also, the block-processing of the data means 2% of the signal will be subjected to underestimation due to the settling time of the angular filter (see 2.1.5), this could however be improved by modifying the data-model to use documents of longer time-span. Given improvements in measurement accuracy, this type of application could serve as a practical quick-assessment tool for analysing measurements, not requiring technical expertise in engineering or signal processing. However, while this work focused on on-line data-visualization, access to the raw data for local analysis and/or more advanced processing should be considered in the future to accommodate the requirements of realistic measurements of longer duration.

4.1. Limitations

Limitations were established prior to development. These consisted of developing the prototype system using a pre-determined set of sensors models as described in 2.1.1 and 2.2.1 (see Appendix B & C for additional specifications). No large or quantitative validations were either to be performed. Lastly, for the online cloud storage services, freely-available services were used.

5. Conclusion

A prototype system for measuring and visualizing forearm load using a smartphone, wearable sensors and IoT technology was developed in this work. Testing under controlled conditions indicated that muscular rest can be measured and classified according to suggested risk thresholds. The method of angular measurement was difficult to implement because of lacking inter-sensor alignment in the horizontal plane, as well as uncertainties in the Bluetooth protocol.

Future work should focus on the IMU:s and look to further develop a method of correcting the relative angle error, as well as investigating accurate time synchronization of the two sensors. Alternatively, deriving angular velocities directly from the IMU gyroscopes could be investigated.

With further work including improved accuracy and extended testing, the system could provide an easy-to-use measurement method in the field of ergonomics. This could make exposure quantification in the working environment more available, thereby lowering the risk for WRMD, reduce the associated financial cost, and above all, prevent individual suffering.

References

- [1] Office of National Statistics, "www.ons.gov.uk," 2016. [Online]. Available: <https://www.ons.gov.uk/employmentandlabourmarket/peopleinwork/labourproductivity/articles/sicknessabsenceinthelabourmarket/2016>. [Accessed 18 05 2018].
- [2] Arbetmiljöverket, "Occupational accidents and work-related diseases (Arbetsmiljöstatistik Rapport 2016:1)," Arbetsmiljöverket, 2016.
- [3] Safe Work Australia, "www.safeworkaustralia.gov.au," 2017. [Online]. Available: <https://www.safeworkaustralia.gov.au/statistics-and-research/statistics/disease-and-injuries/disease-and-injury-statistics-type>. [Accessed 18 05 2018].
- [4] K. Eliason, P. Palm, T. Nyman and M. Forsman, "Inter- and intra- observer reliability of risk assessment of repetitive work without an explicit method," *Applied Ergonomics*, vol. 62, pp. 1-8, 2017.
- [5] E. Takala, I. Pekhonon, M. Forsman, G. Hansson, S. Mathiassen, W. Neumann, G. Sjøgaard, K. Veiersted, R. Westgaard and J. Winkel, "Systematic Evaluation of Observational Methods Assessing Biomechanical Exposures at Work," *Scandinavian Journal of Work, Environment & Health*, vol. 36, no. 1, pp. 3-24, 2010.
- [6] I. Balogh, K. Ohlsson, C. Nordander, S. Skerfving and G. Å. Hansson, "Precision of measurements of physical workload during standardized manual handling part III: Goniometry of the wrists," *Journal of Electromyography and Kinesiology*, vol. 19, no. 5, pp. 1005 - 1012, 2009.
- [7] A. Murgia, P. J. Kyberd, P. H. Chappell and C. Light, "Marker placement to describe the wrist movements during activities of daily living in cyclical tasks," *Clinical Biomechanics*, vol. 19, no. 3, pp. 248 - 254, 2004.
- [8] P. Jonsson and P. W. Johnson, "Comparison of measurement accuracy between two types of wrist goniometer systems," *Applied Ergonomics*, vol. 32, no. 6, pp. 599-607, 2001.
- [9] C. Nordander, K. Ohlsson, I. Åkesson, i. Arvidsson, I. Balogh, G.-Å. Hansson, U. Strömberg, R. Rittner and S. Skerfving, "Exposure-response relationships in work-related musculoskeletal disorders in elbows and hands – A synthesis of group-level data on exposure and response obtained using uniform methods of data collection," *Applied Ergonomics*, vol. 44, pp. 241-253, 2013.
- [10] I. Arvidsson, C. Dahlqvist, H. Enquist and C. Nordander, "Åtgärdsnivåer mot belastningsskada," Arbets- och Miljömedicin Syd, 2017.

- [11] M. Forsman, E. Bernmark, B. Nilsson, S. Pousette and M. Svend Erik, "Participative development of packages in the food industry – evaluation of ergonomics and productivity by objective measurements," *Work*, vol. 41, pp. 1751-1755, 2012.
- [12] FORTE, "forte.se," 27 09 2017. [Online]. Available: <https://forte.se/app/uploads/2017/09/projektbidrag-juniorforskarbidrag-postdokbidrag-2017-09-27.pdf>. [Accessed 26 04 2018].
- [13] G.-Å. Hansson, I. Balogh, K. Ohlsson, L. Rylander and S. Skerfving, "Goniometer Measurement and Computer Analysis of Wrist Angles and Movements Applied to Occupational Repetitive Work," *J Electromyography Kinesiolog*, vol. 6, no. 1, pp. 23-35, 1996.
- [14] L. Perumal, "Euler angles: conversion of arbitrary rotation sequences to specific rotation sequence," *Computer Animation and Virtual Worlds*, vol. 25 , no. 5 - 6, pp. 521 - 529, 2013.
- [15] LP Research, "LP Research Motion Sensor Reference Manual v1.3.4," LP Research, 2018.
- [16] "IMU Core Sensor Fusion," [Online]. Available: <https://www.lp-research.com/imucore-sensor-fusion/>. [Accessed 27 04 2018].
- [17] D. Borgström, "Validation of a Smart shirt for tracking work postures of the trunk," KTH, Stockholm, 2018.
- [18] R. Vitali, S. Cain, R. McGinnis, A. Zaferiou, L. Ojeda, S. Davidsson and N. Perkin, "Method for Estimating Three-Dimensional Knee rotation using two imus," *Sensors*, vol. 17 , no. 9, 2017.
- [19] Biometrics Ltd, "biometricsltd, "Electrogoniometer and Torsiometer Specifications"," [Online]. Available: <http://www.biometricsltd.com/goniometer.htm>. [Accessed 18 5 2018].
- [20] T. Dauncey, H. Sing and J. Dias, "Electrogoniometer measurement and directional analysis of wrist angles and movements during the Sollerman hand function test," *Journal of Hand Therapy*, vol. 30, pp. 328-336, 2017.
- [21] Shimmer, "Shimmer Java/Android API," [Online]. Available: <http://www.shimmersensing.com/products/shimmer-android-id>. [Accessed 1 april 2018].
- [22] C. Nordander, I. Balogh, S. Mathiassen, K. Ohlsson, J. Unge, S. Skerfving and G. Hansson, "Precision of measurements of physical workload during standardised manual handling.Part I: Surface electromyography of m. trapezius, m. infraspinatus and the forearm extensors," *Journal of Electromyography and Kinesiology*, vol. 14, pp. 443-454, 2004.

- [23] J. G. Simonsen, C. Dahlqvist, H. Enquist, C. Nordander, A. Axmon and I. Arvidsson, "Assessments of Physical Workload in Sonography Tasks Using Inclinometry, Goniometry, and Electromyograph," *Safety and Health at Work*, pp. 1 - 8, 2017.
- [24] R. G. Mello, L. F. Oliveira and J. Nadal, "Digital Butterworth filter for subtracting noise from low magnitude surface electromyogram," *Computer methods and programs in biomedicine*, vol. 87, pp. 28-35, 2007.
- [25] "MathWorks Documentation: filfilt zero-phase digital filtering," [Online]. Available: <https://se.mathworks.com/help/signal/ref/filffilt.html>. [Accessed 16 05 2018].
- [26] "Shimmer EMG User Guide Rev. 1.12," Shimmer, 2017.
- [27] H. Ghapanchizadeh, S. A. Ahmad and A. Juraiza Ishak, "Recommended Surface EMG Electrode Position for Wrist Extension and Flexion," in *2015 IEEE Student Symposium in Biomedical Engineering & Sciences*, 2015.
- [28] "MongoDB Manual 3.6 Reference: MongoDB Limits and Thresholds," [Online]. Available: <https://docs.mongodb.com/manual/reference/limits/>. [Accessed 26 04 2018].
- [29] N. Q. Mehmood, R. Culmone and L. Mostarda, "Modeling temporal aspects of sensor data for MongoDB NoSQL database," *Journal of Big Data*, vol. 4, no. 8, 2017.
- [30] "Schema design for time series data in MongoDB," 30 10 2013. [Online]. Available: <https://www.mongodb.com/blog/post/schema-design-for-time-series-data-in-mongodb>. [Accessed 26 04 2018].
- [31] A. M. Sabatini, "Estimating Three-Dimensional Orientation of Human Body Parts by Inertial/Magnetic Sensing," *Sensors*, pp. 1489-1525, 2011.
- [32] K. Lebel, P. Boissy, M. Hamel and C. Duval, "Inertial Measures of Motion for Clinical Biomechanics: Comparative Assessment of Accuracy under Controlled Conditions - Effect of Velocity," *PLOS ONE*, vol. 8, no. 11, 2013.
- [33] E. Palermo, S. Rossi, F. Patané, Cappa and P, "Experimental evaluation of indoor magnetic distortion effects on gait analysis performed with wearable inertial sensors," *Physiological Measurement*, pp. 399-415, 2014.
- [34] W. de Vries, H. Veeger, C. Baten and F. van der Helm, "Magnetic distortion in motion labs, implications for validating inertial magnetic sensors," *Gait and posture*, vol. 29, no. 4, pp. 535-541, 2009.
- [35] C. L. Kendall and E. D. Lemaire, "Effect of Mobility Devices on Orientation Sensors that Contain Mangetometers," *J Rehabil Res Dev*, vol. 46, no. 7, pp. 957-962, 2009.

- [36] E. Farella, L. Benini and B. Riccó, "MOCA: A Low-Power, Low-Cost Motion Capture System," *Advances in Multimedia*, 2007.
- [37] B. Buchholz and H. Wellman, "Practical Operation of a Biaxial Goniometer at the Wrist Joint," *Human Factors*, vol. 39, no. 1, pp. 119 - 129, 1997.
- [38] G. Å. Hansson, I. Balogh, K. Ohlsson and S. Skerfving, "Measurements of wrist and forearm positions and movements: effect of, and compensation for, goniometer crosstalk," *Journal of Electromyography and Kinesiology*, vol. 14, pp. 355-367, 2004.
- [39] S. Kim and M. A. Nussbaum, "Performance evaluation of a wearable inertial motion capture system for capturing physical exposures during manual material handling tasks," *Ergonomics*, vol. 56, no. 2, pp. 1366 - 1547, 2013.
- [40] B. Huyghe, J. Doutreloigne and J. Vanfleteren, "A Wireless Sensor Network Protocol for an Inertial Motion Tracking System," *Wireless Personal Communications*, vol. 71, no. 3, p. 1961-1975 , 2012.
- [41] J. Wåhslen, "Multi-Sensor Data Synchronization using Mobile Phones," KTH, 2013.
- [42] M. Alvaro, R. Casas, J. Ramos, V. Coarasa, A. Asensio and M. Obaidat, "Synchronization of multihop wireless sensor networks at the application layer," *IEEE Wireless Communications*, vol. 18, no. 1, 2011.
- [43] J. C. F. De Winter, "Using the Student's "t"-Test with Extremely Small Sample Sizes," *Practical Assessment, Research & Evaluation*, vol. 18, no. 10, 2013.
- [44] C. J. Ives and J. K. Wigglesworth, "Sampling rate effects on surface EMG timing and amplitude measures," *Clinical Biomechanics*, vol. 18, pp. 543-552, 2003.
- [45] A. J. Bianchi and M. Queiroz, "On the performance of real-time DSP on Android devices," in *SMC 2012, Sound and Music Computing Conference*, 2012.
- [46] D. Laidig, P. Müller and T. Seel, "Automatic anatomical calibration for IMU-based elbow angle measurement in disturbed magnetic fields," *Current Directions in Biomedical Engineering*, vol. 3, no. 2, pp. 167-170, 2017.
- [47] T. Seel, J. Raisch and T. Schauer, "IMU-Based Joint Angle Measurement for Gait Analysis," *Sensors*, vol. 14, no. 4, pp. 6891-6909, 2014.
- [48] J. Favrea, B. Jollesb, R. Aissaouic and K. Aminiana, "Ambulatory measurement of 3D knee joint angle," *Journal of Biomechanics*, vol. 41, pp. 1029-1035, 2008.
- [49] J. Chow, "Statistical Sensor Fusion of A 9-DOF MEMS IMU for Indoor Navigation," in *The International Archives of the Photogrammetry, Remote Sensing and Spatial*

- [50] G. Ligorio and A. Sabatini, "Dealing with Magnetic Disturbances in Human Motion Capture: A Survey of Techniques," *Micromachines*, vol. 7, no. 3, 2016.
- [51] A. Corbellini, C. Mateos, A. Zunino, D. Godoy and S. Schiaffino, "Persisting big-data: The NoSQL landscape," *Information Systems*, vol. 63, pp. 1-23, 2017.
- [52] J. Van der Veen, B. Vand der Waaij and R. Meijer, "Sensor Data Storage Performance: SQL or NoSQL, Physical or Virtual," in *2012 IEEE Fifth International Conference on Cloud Computing*, 2012.
- [53] E.-P. Takala and R. Toivonen, "Placement of forearm surface EMG electrodes in the assessment of hand loading in manual tasks," *Ergonomics*, vol. 56, no. 7, pp. 1159-1166, 2013.
- [54] C. De Luca, D. Gilmore, M. Kuznetsov and S. Roy, "Filtering the surface EMG signal: Movement artifact and baseline noise contamination," *Journal of Biomechanics*, vol. 43, pp. 1573-1579, 2010.
- [55] J. Galiana-Merino, D. Ruiz-Fernandez and J. Martinez-Espla, "Power line interference filtering on surface electromyography based on the stationary wavelet packet transform," *computer methods and programs in biomedicine*, pp. 338-346, 2013.
- [56] G. Hägg, A. Luttman and M. Jäger, "Methodologies for evaluating electromyographic field data in ergonomics," *Journal of Electromyography and Kinesiology*, pp. 301-312, 2000.

Appendix A: State of the Art Report

State of the Art Report: HL205X Master Thesis

Acquisition and Online Visualization of IMU and EMG Sensor Data for Assessment of Wrist Load

Axel Hult

Daniel M. Chang

Mars 2018

Content

Acronyms and Abbreviations	c
1.1. Introduction	- 1 -
1.2. Wrist Ergonomics	- 1 -
1.3. Quantifying Exposure.....	- 3 -
1.4. Inertial Measurement Unit	- 4 -
1.5. Rotations in R^3	- 5 -
1.6. Electromyography	- 6 -
1.7. Cloud computing.....	- 7 -
1.8. Internet of Things.....	- 7 -
1.9. IoT Communication.....	- 8 -
1.10. Data Storage.....	- 8 -
Literature.....	- 10 -

Acronyms and Abbreviations

EMG	<i>Electromyography</i>
IMU	<i>Inertial Measurement Unit</i>
IOT	<i>Internet Of Things</i>
JSON	<i>JavaScript Object Notation</i>
MVC	<i>Maximum voluntary contraction</i>
MQTT	<i>Message Queuing Telemetry Transport</i>
SQL	<i>Structured Query Language</i>
WRMD	<i>Work-related musculoskeletal disorders</i>

1.1. Introduction

Sustaining healthy and ergonomical working environments can be a crucial step in maintaining employee wellbeing and efficiency. Work-related injuries and sickness can otherwise create continuous expense in the form worker absence and healthcare costs. In the UK alone, 137.3 million working days were reported lost in 2016 due to sickness or injury [1]. The figure is however, a part of a declining trend which was at its peak in 1995-1999 with 180 million days lost per year [1]. To further prevent the expenses and discomfort generated by work-related sickness and injuries an understanding of its causes is necessary. A leading cause of worker absence is due to musculoskeletal disorders [1, 2, 3, 4, 5]. Work-related Musculoskeletal Disorders or WRMDs, can be defined as disorders concerning *muscles, nerves, tendons, ligaments, joints, cartilage, blood vessels, or spinal disks in the neck, shoulder, elbow, forearm, wrist, hand, abdomen (hernia only), back, knee, ankle, and foot associated with exposure to risk factors*" [2].

During the year of 2016, a total of 30.8 million working days were lost in the UK due to WRMDs, which stands for 18 % of the total reports. Similar values can also be seen internationally [3, 5, 4], where in countries such as the US, WRMDs stood for 31% of the reports in 2015 [5]. Looking at the globally reported WRMDs, wrist and hand related reports are among the most prominent [3, 4]. In the US, wrist and hand disorders are the third most reported WRMDs [5], while in the UK they stand as the second most prominent [2]. With this high global prevalence of hand and wrist related WRMDs, awareness of the matter and its preventions is being raised. Preventing these disorders would lower the damages and costs that come from harmful working environments. However, due the wide variety of occupations and working environments, a better understanding of how wrists and hands are used is required.

1.2. Wrist Ergonomics

By following studies of wrist related complications in working environments, flexion and extension of the wrist has been shown to correlate with documented wrist related complaints [6]. The two actions are seen as a risk factors and are analyzed by ergonomists and researchers when investigating WRMD [6]. The human wrist is composed of proximal and distal carpal bones (carpals) that with carpal ligaments connect the radial and ulnar bones to the meta carpals (see figure 1). Muscular forces are perpetuated through muscular tendons alongside the median nerve inside of the carpal tunnel (see figure 2). Flexion and extension of the hand relative to the forearm is typically possible in the range of 100-140 degrees while abduction and adduction is typically possible in the range of 50-60 degrees. Wrist-angle analysis is typically performed using a simplified model where the 3rd metacarpal bone (see figure 1) is set as the center of a coordinate system representing the hand as a rigid mass moving with respect to the forearm [7].

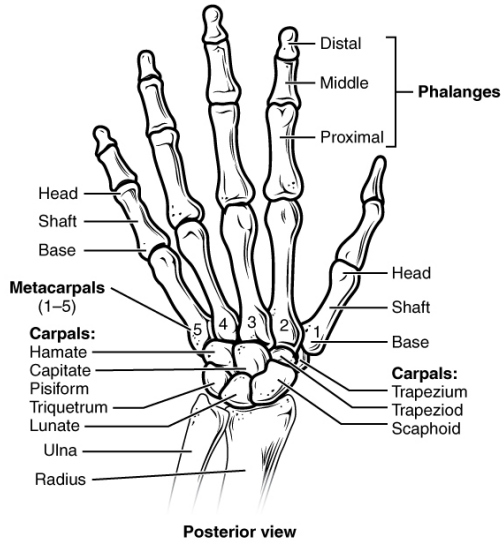


Figure 1. Skeletal anatomy of the wrist [57]

Repetitive movements in combination with high force have in addition to absolute wrist angles been shown to increase the risk of developing WRMD. The majority of repetitive motion injuries of the upper limb affect either the wrist or hand [6, 9]. Repetitive tasks have been described as a general risk factor for WRMD, even at light loads. [10]. Separating the effect of repetition and force is not trivial. However, there is agreement that the combination of high force and repetition carries an especially increased risk of WRMD [9, 10, 11]. Carpal tunnel syndrome is a specific disorder of the hand where the median nerve is compressed by increased pressure on the carpal tunnel (see figure 2). Substantial evidence suggests that repetitive flexion or extension together with a forceful grip are risk factors for developing carpal tunnel syndrome [12].

Forceful gripping has also been associated to WRMD of wrist and hand. Increased pressure on the carpal tunnel from heavy palmar loads have been demonstrated in cadaver studies, suggesting a possible cause [13]. Because grip force generally increases with external weight, it is therefore likely that higher external gripping loads could increase the risk factor for WRMD [10]. Much like griping actions, carpal tunnel syndrome as well as medial and lateral epicondylitis (Tennis Elbow), have also been associated with wrist flexion and extension [6, 10]. Ulnar and radial deviations of the wrist have been linked to carpal tunnel syndrome, tenosynovitis of the thumb abductors and lateral epicondylitis [10] and musculoskeletal disorders of the wrist in general [14]. Further developments include neurovascular disorders like reflex sympathetic dystrophy and Raynaud's syndrome. The resulting symptoms may include muscular spasms and cramping of the forearm and hand [9]. There are also a number of non-specific conditions characterized by pain, discomfort and fatigue [9, 15].

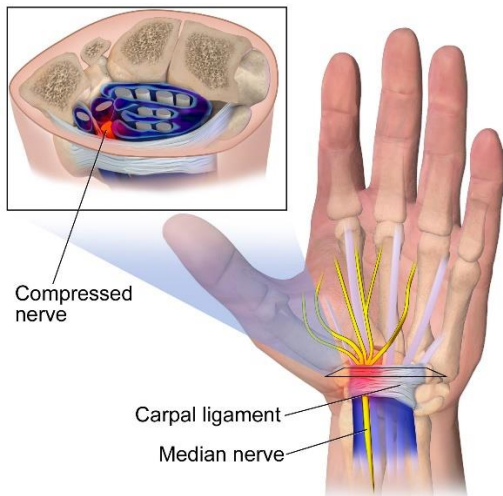


Figure 2. Strain exhibited on the median nerve during carpal tunnel syndrome [58].

Among the recent studies done on wrist ergonomics, a concern in the wrist angular velocities of workers have appeared. The studies demonstrate how angular velocities could be a reliable parameter for assigning risk groups [11]. Similar studies have shown that the velocity may even be a more reliable method compared to absolute angles, demonstrating a stronger correlation to WRMD. [6]. The combination of angular velocity, force and repetitiveness could be important parameters to investigate as they all correlate with the occurrence of wrist disorders.

Among the different risk factors related to WRMDs in the wrist, an important factor to be taken into consideration is rest. Opposite to the previously mentioned correlation between WRMD and angle, velocity or force, increased muscular rest has demonstrated to decrease wrist related disorders [17]. When investigating the development of WRDMs, the amount of rest could therefore be included to further understand working environments.

1.3. Quantifying Exposure

Field methods used for quantifying exposures in ergonomics include questionnaires, video analysis and direct measurements [18]. Observational assessments are often performed without a systematic method which produce low-reliability and inaccurate estimates [19] causing ergonomists to often rate the same exposure differently among themselves and others [20]. For the wrist and hand specifically, observatory measurements are especially inaccurate [21] and direct measurement of force and velocity generally provides the most accurate method of quantifying exposure [18].

It was with the implementation of electronic measurement systems that consistent methods were developed [22]. In the current stage of development, electronic goniometers are generally used as the golden standard when measuring wrist motion [23]. Goniometers are devices mounted along the joint of interest which converts the mechanical bending to an electrical signal [24]. They allow wrist data to be sampled over an extended period of time, which can later be used in biomechanical models to estimate more complex measures like joint torques [10] and angular velocities [6].

However, limitations presented by the current electronic goniometer exists due to their size and weight [25]. This might affect the behavior of the subject being measured. Also, the device cost and the associated complexity of dataloggers and dedicated software have limited their use to research applications. There is a need for alternative measurement methods with small and wireless sensors, that are cheap and easy to use.

Alternative methods for joint-angle measurements are optical systems that use visual markers placed on the body that are then tracked with cameras [26, 27]. The method accurately measures angles and movements with limited obstruction. However, the method restricts the subject to remain in the visual range of the cameras, and the visual markers must not be covered during movement [27]. Applying visual trackers in working environments could cause significant restrictions in working environments. Further alternatives such as inclinometers [28] or accelerometers [29] provide with wireless and small systems that measures the gravitational force of the earth. By positioning 3 accelerometers orthogonal to each other, the sensors may detect pitch and roll rotations, represented in figure 3. These rotations are inclinations parallel to the gravitational field. However, rotations along the horizontal plane of the earth or yaw-rotations will remain undetected [30]. This limits the sensors use in places such as office environments with computer-related tasks requiring frequent rotations along a horizontal surface.

By expanding the idea of accelerometers, Inertial Measuring Units(IMUs) that combine sensor data from several complementary sensors provide with a more versatile tracking option. Studies have demonstrated the accuracy of its use in joint angle measurements [31]. And with the implementation of MEMS (Micro-Electro-Mechanical Systems) sensors, the size of the units may also remain minimal, resulting in less movement restrictions on subjects [31, 32].

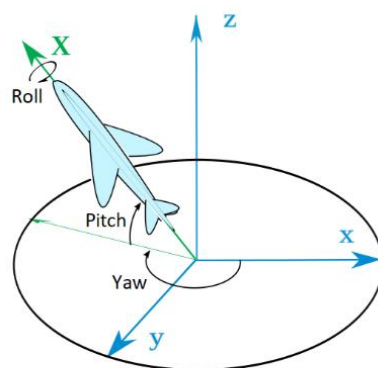


Figure 3. Representations of possible rotations in a 3D plane [59].

1.4. Inertial Measurement Unit

In an IMU, accelerometers, gyroscopes and magnetometers are integrated into one measuring system [34]. However, each individual sensor exhibit restrictions and become

unreliable in certain situations. The rotation of an IMU can be calculated by integrating the angular velocities generated from the gyroscopes [30]. However, with the use gyroscopes, a source of errors is included. Undesired shifts in the integration may produce a drift that builds up with prolonged use [35]. By including accelerometers that rely on a relatively constant parameter, the drift in pitch and roll generated by the gyroscopes can be corrected [34]. Yaw drift can be corrected by magnetometers that utilizes the magnetic flux from earth's magnetic field. To properly correct the yaw drift of the gyroscope a static reference frame must be determined from the magnetic field [35]. However, unlike gravitational forces measured by accelerometers, the magnetic fields measured by magnetometers can be inconsistent [34]. This can be caused by being in proximity to certain materials and electrical equipment, and becomes especially problematic indoors [36].

To correctly track rotations from IMU-data, the limitations of all sensors has to be considered. When forming the sensory information into orientations, inconsistent or contradicting readings may appear from the different sensors [34]. The fusion requires appropriate filters to be implemented to maintain a consistent and reliable output. Kalman filters are commonly implemented for this purpose [37]. These are recursive algorithms that can estimate the orientation based on a stochastic model, with the data from the IMU sensors as the input [36].

Flexion-extension of a body joint can be estimated with a pair of IMUs located on each side of the joint [32]. To retrieve the angle between the sensors, one approach is to simply find the difference of the integrated angular rates of the two sensors. Other methods rely on estimates of the absolute orientation of the two sensors with respect to their reference frames. With known reference systems to both sensors, these orientations can then be transformed into a common reference system and the relative angle between them can be calculated [32]. The same methods could possibly be extended to movement in other anatomical planes, i.e. abduction/adduction and inversion/eversion. [32]. Similar methods have been used for 2-dimensional movements incorporating both flexion/extension and pronation/supination of the elbow joint were compensation mechanisms for magnetic field disturbances and sensor placements is incorporated [38]. Additional studies demonstrate the capabilities of Joint-angle measurements using several IMUs on the knee joint [39, 40]

1.5. Rotations in \mathbb{R}^3

The sensory fusion in IMUs aim to provide estimates of the orientation of the device in 3D-space. Three-dimensional orientations and rotations can be represented in different models [41]. Euler angles is a conceptually easy model to understand and represents complex rotations as a sequence of three elementary rotations [42]. However, Euler angles are of limited use when measuring unconstrained rotations. A mathematical singularity can occur in certain orientations leading to a loss of one degree of freedom [42]. This phenomenon is more commonly known as gimbal lock [43, 44]. In these cases

where Euler angles are insufficient, quaternions can be used instead. Quaternions avoid gimbal-lock by representing rotations using a four-dimensional parametrization [43]. Quaternions can be described as a generalization of the complex numbers, and can be expressed in the form [41]:

$$\mathbf{q} = q_1 + (q_2 \mathbf{i} + q_3 \mathbf{j} + q_4 \mathbf{k})$$

where q_1 is called the real- [45] or scalar-part [41] and $(q_2 \mathbf{i} + q_3 \mathbf{j} + q_4 \mathbf{k})$ is called the imaginary- [45] or vector-part [41]. Quaternions with a scalar-part equal to zero are called vector- [41] or pure-quaternions [42] and represent vectors in the R3-space made up by the complex numbers \mathbf{i} , \mathbf{j} and \mathbf{k} [41].

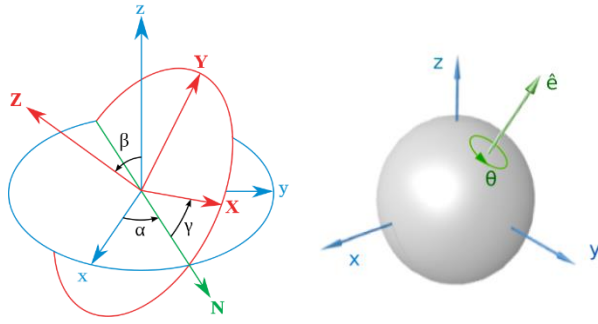


Figure 2. R3-rotations can be described by Euler-angles(left) [60] as well as axis-angle representation (right) [61].

Euler's rotation theorem states that any rotation can be described with an angle (ω) and a respective axis of rotation (see figure 4b). With this, a given quaternion $\mathbf{q} = \cos\left(\frac{\omega}{2}\right) + \mathbf{a} \sin\left(\frac{\omega}{2}\right)$, where $\|\mathbf{a}\| = 1$, the rotation of a vector $\mathbf{x} \in \mathbb{R}^3$ to a vector $\mathbf{x}' \in \mathbb{R}^3$ is described by the operation:

$$\mathbf{x}' = \mathbf{q} \otimes \mathbf{x} \otimes \mathbf{q}^*$$

where \otimes describes quaternion-multiplication and \mathbf{q}^* is the conjugate of \mathbf{q} [62]. This operation is equivalent to axis-angle representation of rotation $R(\omega, \mathbf{a})$ describing a rotation ω along the rotation-axis \mathbf{a} [45]. Using the same formalism, composite rotations can be described by [42]:

$${}^C_A \mathbf{q} = {}^C_B \mathbf{q} \otimes {}^B_A \mathbf{q}$$

where ${}^A_C \mathbf{q}$ denotes the rotation from A to C.

In summary, quaternions are a set of four-dimensional numbers and associated operations that provide a singularity free, computationally efficient and accurate [41] way of representing arbitrary rotations in 3D space.

1.6. Electromyography

To estimate the force experienced by the body electromyography (EMG) can be used. EMG measures the electric activity of muscles and have been used in the field of ergonomics for over 50 years [48].

Force is believed to be a risk factors in developing WRMD, and has been estimated using various techniques including dynamometers, direct measurement of weight of objects [9], strain gauges and even thermography [10]. Muscle activity measured with EMG has both been suggested as a relevant measure on its own [11] but has also been used as estimation of force due to the correlation between the two parameters [18]. The information from the EMG can thus be interpreted both from a biomechanical- (forces and torques) or physiological (activation and fatigue) point of view, both of which are relevant in ergonomics [48].

When force is the desired parameter a calibration curve must be established between the signal amplitude and a known force, a procedure which involves several sources of error [48]. The relationship between the EMG-amplitude and the generated force is also influenced by a number of different factors including limb position, posture and working techniques [11, 49].

Needle EMG pinpointing specific muscle is practically challenging, and so surface-electrode EMG is used instead. Using surface-electrodes has some possible sources of error including electrode positioning relative to the muscle of interest, and skin stretching [11].

Muscle activity is commonly represented by the Root-Mean-Square amplitude of the EMG-waveform (rms-EMG), typically using time-windows in the range 100-400 milliseconds [14, 18, 48]. Spectral parameters can also be derived for analysis in the frequency domain [48].

Unlike orientations retrieved from IMU sensors, the readings from the EMG are not normalized and the signal amplitude can vary considerably. A normalization procedure is necessary. Percent of Maximum Voluntary Contraction (% MVC) is often used in as a reference for EMG-data for an individual [14, 18]. For example, rms-EMG at 15 %MVC have been used as the mean acceptable contraction intensity for work during extended time [11] and muscular rest has been defined as rms-EMG signals below 0.5 % of MVC [6]. This rest-measure has been applied to EMG-signals from the forearm extensor muscles to quantify wrist stress in many different occupations [6, 50].

1.7. Cloud computing

The National Institute of Standards and Technology (NIST) defines cloud computing as:

“...a model for enabling ubiquitous, convenient, on-demand network access to a shared pool of configurable computing resources (e.g., networks, servers, storage, applications, and services) that can be rapidly provisioned and released with minimal management effort or service provider interaction” [51].

The concept of cloud computing can be further divided into the three different service models Software-as-a-Service (SaaS), Platform-as-a-Service (PaaS) and Infrastructure-as-a-Service (IaaS) [51, 52]. The SaaS-model provide access to pre-built online applications and or databases, typical examples are public applications like email or social networks [53], whereas the IaaS-model only provides the hardware resources (network, storage etc.) with all software development and configuration left to the customer [52]. IaaS is provided by companies like Amazon, IBM and Microsoft [53].

The PaaS-model offers a computing platform and tools for clients to develop their own applications while the management of the underlying platform and infrastructure is

maintained by the provider. Using cloud-computing and a PaaS for application development can be beneficial in terms of reduced costs and complexity from not having to manage the underlying IT-structure [54, 55]. Also, using readily available software components provided by the PaaS allows faster construction of new applications [52].

1.8. Internet of Things

The Internet of Things (IoT) is a rapidly emerging paradigm in information technology describing the connection of physical and virtual things to global networks [48] and communication among smart objects [49]. The use IoT technology in healthcare will likely have substantial effect on society [50], and opens up the possibility of things like continuous pervasive monitoring using networks of sensors connected to the cloud [51]. The general architecture of sensor-based IoT systems can be described by four layers. The sensing layers consist of sensors and wearable devices for collecting data. The network layer is responsible for sensor interconnectivity and collection and transmission of the data. The processing layer handles computation of the collected data and the application layer provides the service and interface to the end user. [48]. An IoT platform combining wearable technologies, data analytics and ergonomics could promote a healthy working life by allowing pervasive monitoring, early detection and warnings as well as risk assessments and self-management by the individual employee [52].

1.9. IoT Communication

Traditional communication protocols typically do not adhere to the constrained requirements on IoT devices including small computational capabilities, low power consumption [53] and large-systems with decentralized communication and a high degree of scalability [49]. IoT protocols typically support a publish-subscribe pattern where a sender publishes messages to a server, which forwards messages to a receiver subscribing to the server. This is in contrast to the request-response pattern often used for communication on the web [54]. There are a number of different protocols used for IoT communication, with three of the most popular ones being COAP, MQTT and AMQP [53, 54]. MQTT is a lightweight opensource protocol built on top of the standard internet protocol TCP [55] designed to be simple and easy to implement [56]. It uses the publish-subscribe model and supports different levels of quality of service for choosing the transmission-reliability. MQTT have found extensive use in IoT application and is used and is supported and used by a large number of organizations [63].

JavaScript Object Notation (JSON) is a popular data format used on the web [65]. JSON has largely replaced XML on the web because of the smaller overhead and the fact that it is natively supported by the JavaScript language used by web-browsers [66]. JSON stores data as simple key-value pairs which can be a number of different types including numbers, strings arrays and other JSON-documents. This format makes JSON easily readable by both machines and humans [65].

```

{
  "name": "Axel",
  "hobbies": ["Fishing", "running", "reading"],
  "vehicles": {
    "bicycle": {
      "Tires": 2,
      "frame": "26 inch"
    },
    "boat": {
      "sails": 2,
      "length": 30
    }
  }
}

```

Figure 3. Example of JSON-formatted data. A key-value pair (*name*), a String-array (*hobbies*) and a document (*vehicles*) with subdocuments.

1.10. Data Storage

With the development of the IoT technologies discussed above the need for storing large amounts of varying data increase rapidly [67]. Data has traditionally been stored in relational databases. These are characterized by well-structured data and fixed storing schema, based on data-models originally developed in the 1970's [68]. Relational databases typically store data as a set of tables of rows and columns and allows access and manipulation of data using Structured Query Language (SQL) [57]. However, because of the underlying design principle of many relational databases, favoring consistency and availability over partitioning of data [58], they are often restricted in achieving efficient processing, parallelization and scalability needed in facing the challenges of massive and diverse amounts of data associated with modern IoT applications. [59, 60].

NoSQL is a term applied to a type of database of growing popularity, trying to solve some of these problems [58]. NoSQL databases are generally unstructured in the sense that they do not have or enforce a fixed schema [59, 61]. NoSQL databases are characterized by their good ability to scale horizontally, meaning that capacity can be increased through addition of additional nodes instead of increasing the resources of a single node [62]. This is implemented using techniques like sharding where data is divided into individual partitions and replication where the same data is available on several servers in order to achieve increased throughput and availability [61]. Horizontal scaling make NoSQL databases well suited for IoT and cloud computing applications [60] although it should be pointed out that some relational databases also support these features [61].

Furthermore the flexible data schema, good performance [60] ease of use without the need to learn SQL [59], fast and easy deployment to a cluster [61] and absence of requirements of predefining relational model or datatypes [63] makes NoSQL databases a good alternative for prototyping IoT applications.

The diagram illustrates the mapping between two relational database tables and a single document database collection. On the left, there are two tables: 'Students Table' and 'Grades Table'. The 'Students Table' has columns: Key, Name, Age, School, and Grades. It contains two rows: one for student 123 (Axel, 25, KTH, *) and one for student 456 (Danie, 23, KTH, *). An arrow points from this table to the 'Student collection' on the right. The 'Student collection' is a table with columns: Key and value. It contains two documents. Document 123 corresponds to student 123 and contains fields: Name: Axel, Age: 25, School: KTH, and Grades: Course A: 5, Course B: 5, Course C: 5. Document 456 corresponds to student 456 and contains fields: Name: Daniel, Age: 23, School: KTH, and Grades: Course A: 1, Course B: 3, Course C: 1.

Students Table				
Key	Name	Age	School	Grades
123	Axel	25	KTH	*
456	Danie	23	KTH	*

Grades Table			
Key	Course A	Course B	Course C
123	5	5	5
456	1	3	1

Student collection	
Key	value
123	Name: Axel Age: 25 School: KTH Grades: Course A: 5 Course B: 5 Course C: 5
456	Name: Daniel Age: 23 School: KTH Grades: Course A: 1 Course B: 3 Course C: 1

Figure 4. Simplified example of a different database types.

Left: A Relational database with two different tables. Right: A document database with one collection.
A document in a NoSQL database can be considered equivalent to a row in a relational database [66].

NoSQL databases can be divided into the four main groups including key-value-, column-, graph and document databases [59, 61]. Document databases offer the most general model of storage [62]. Documents are typically JSON-formatted sets of data of arbitrary complexity and content [60]. A document can contain single values, lists and sub-documents, and the type of data and schema can be changed dynamically. Documents of similar content are grouped into collections [62]. MongoDB is one example of an open-source NoSQL document-databases that stores data in the form of key-value pairs using BSON-format (binary-JSON) [58].

References

- [1] ONS, "www.ons.gov.uk," 2016. [Online]. Available: <https://www.ons.gov.uk/employmentandlabourmarket/peopleinwork/labourproductivity/articles/sicknessabsenceinthelabourmarket/2016>. [USED 2018 02 20].
- [2] Health and Safety Executive, "http://www.hse.gov.uk," 2017. [Online]. Available: <http://www.hse.gov.uk/statistics/causdis/musculoskeletal/msd.pdf>. [USED 2018 02 20].
- [3] Arbetmiljöverket, "www.av.se," 2016. [Online]. Available: <https://www.av.se/globalassets/filer/statistik/arbetsskador-2015/arbetsmiljostatistik-arbetsskador-2015-rapport-2016-01.pdf?hl=arbetsskador%20statistik> [USED 2018 02 20].
- [4] Safe Work Australia, "www.safeworkaustralia.gov.au," 2017. [Online]. Available: <https://www.safeworkaustralia.gov.au/statistics-and-research/statistics/disease-and-injuries/disease-and-injury-statistics-type>. [USED 2018 02 20].
- [5] Bureau of Labor Statistics, "www.BLS.gov," 2016. [Online]. Available: <https://www.bls.gov/news.release/pdf/osh2.pdf>. [USED 2018 02 20].
- [6] C. Nordander, K. Ohlsson, I. Åkesson, i. Arvidsson, I. Balogh, G.-Å. Hansson, U. Strömberg, R. Rittner och S. Skerfving, "Exposure–response relationships in work-related musculoskeletal disorders in elbows and hands – A synthesis of group-level data on exposure and response obtained using uniform methods of data collection," *ScienceDirekt*, 2013.
- [7] K. D. Oberländer, "Inertial Measurement Unit (IMU) Technology Inverse Kinematics: Joint Considerations and the Maths for Deriving Anatomical Angles," 2015.
- [8] https://commons.wikimedia.org/wiki/File:806_Hand_and_Wrist.jpg, "Hand and Wrist". [USED 2018 02 20].
- [9] A. E. Barr och M. F. Barbe, "Pathophysiological Tissue Changes Associated With Repetitive Movement: A Review of the Evidence," *Physical Therapy*, vol. 82, nr 2, pp. 173-187, 2002.
- [10] J. M. Muggleton, R. Allen och P. Chappell, "Hand and arm injuries associated with repetitive manual work in industry: a review of disorders, risk factors and preventive measures," *Ergonomics*, vol. 42, nr 5, pp. 714-739, 1999.
- [11] J. Malchaire, N. Cock, A. Piette, R. Dutra Leao, M. Lara och F. Amaral, "Relationship between work constraints and the development of

musculoskeletal disorders of the wrist: A prospective study," *International Journal of Industrial Ergonomics*, pp. 471-482, 1997.

- [12] K. T. Palmer, E. C. Harris och D. Coggo, "Carpal tunnel syndrome and its relation to occupation: a systematic literature review," *Occupational Medicine*, vol. 57, pp. 57-66, 2007.
- [13] R. W. McGorry, N. Fallentin, J. H. Andersen, P. J. Keir, T. J. Hansen, G. Pranksy och J.-H. Lin, "Effect of grip type, wrist motion, and resistance level on pressures within the carpal tunnel of normal wrists," *Wiley*, 2014.
- [14] J. B. Malchaire, N. A. Cock och A. R. Robert, "Prevalence of musculoskeletal disorders at the wrist as a function of angles, forces, repetitiveness and movement velocities," *Scand J Work Environ Health*, vol. 22, pp. 176-181, 1996.
- [15] M. Boocock, J. Collier, P. McNair, M. Simmonds, P. Larmer och B. Armstrong, "A Framework for the Classification and Diagnosis of Work-Related Upper Extremity Conditions: Systematic Review," *Seminars in Arthritis and Rheumatism*, vol. 38, nr 4, pp. 296-311, 2009.
- [16] Blausen.com staff (2014). "Medical gallery of Blausen Medical 2014". *WikiJournal of Medicine* 1 (2). DOI:10.15347/wjm/2014.010. ISSN 2002-4436. [USED 2018 02 20].
- [17] G.-Å. Hansson, I. Balogh, K. Ohlsson, L. Granqvist, C. Nordander, I. Arvidsson, I. Åkesson, J. Unge, R. Rittner, U. Strömberg och S. Skerfvin, "Physical workload in various types of work: Part I. Wrist and forearm," *International Journal of Industrial Ergonomic*, p. 221–233, 2009.
- [18] P. Spielholz, B. Silverstein, M. Morgan, H. Checkoway och J. Kaufman, "Comparison of self-report, video observation and direct measurement methods for upper extremity," *Ergonomics*, vol. 44, nr 6, pp. 588-613, 2001.
- [19] K. Eliason, P. Palm, T. Nyman och M. Forsman, "Inter- and intra- observer reliability of risk assessment of repetitive work without an explicit method," *Applied Ergonomics*, pp. 1-8, 2017.
- [20] I.-M. Rhén, N. Balliu och M. Forsman, "OCRA inter-and intra-ergonomist reliability in ten video recorded work tasks," Congress of the IEA, 2015.
- [21] T. e. al, "Systematic evaluation of observational methods assessing biomechanical exposures at workT," *Scandinavian Journal of Work, Environment & Health*, vol. 36, nr 1, pp. 3-24, 2010.
- [22] I. Balogh, K. Ohlsson, C. Nordander, S. Skerfving och G. Å. Hansson, "Precision of measurements of physical workload during standardized manual handling part III: Goniometry of the wrists," *ScienceDirekt*, 2009.

- [23] E. Swarin och G. L. Harrelson, "Measurement in rehabilitation," i *Physical rehabilitation fo the injured athlete*, ELSEVIER, 2012, pp. 67-73.
- [24] G. Hansson, I. Balogh, K. Ohlsson och S. Skerfving, "Measurements of wrist and forearm positions and movements: effect of, and compensation for, goniometer crosstalk," *Journal of Electromyography and Kinesiology*, vol. 14, pp. 355-367, 2004.
- [25] N. Carbonaro, D. M. Gabriele, F. Lorussi, R. Paradosi och D. T. A. De Rossi, "Exploiting Wearable Goniometer Technology for Motion Sensing Gloves," *IEEE*, 2014.
- [26] S. K. Trehan, S. K. Rancy och J. P. H., "Photography-based Method for Measuring Wrist Range of Motion," *Sage journals*, 2016.
- [27] P. F. M. Eichelberger, U. Minder, T. Denton, A. Blasimann, F. Krause och H. Baur, "Analysis of accuracy in optical motion capture – A protocol for laboratory setup evaluation. *Journal of Biomechanics*," Elsevier, pp. 2085-2088, 2016.
- [28] S. Vercelli, F. Sartorio, E. Bravini och G. Ferriero, "DrGoniometer: a reliable smartphone app for joint angle measurement," *BMJ journals*, 2017.
- [29] E. Farella, L. Benini och B. Riccó, "MOCA: A Low-Power, Low-Cost Motion Capture System," *Hindawi*, 2006.
- [30] LP-research, LPMS Reference manual, LP, 2014, p. 8. [USED 2018 02 20].
- [31] P.-C. Hsiao, S.-Y. Yang och B.-S. Lin, "Data glove embedded with 9-axis IMU and force sensing sensors for evaluation of hand function," *IEEE*, 2015.
- [32] T. Seel, J. Raisch och T. Schauer, "IMU-Based Joint Angle Measurement for Gait Analysis," *Sensors*, 2014.
- [33] <https://commons.wikimedia.org/wiki/File:Plane.svg>, "Plane". [USED 2018 02 20].
- [34] S. Zihajehzadeh, D. Loh, T. J. Lee, R. Hoskinson och E. J. Park, "A cascaded Kalman filter-based GPS/MEMS-IMU integration for sports applications," ScienceDirect, 2005.
- [35] LP research, LPMS reference manual, vol. 1.3.4, LP research, 2014, pp. 8-10.
- [36] B. e. al, "Estimating Orientation Using Magnetic and Inertial Sensors and Different Sensor Fusion Approaches: Accuracy Assessment in Manual and Locomotion Tasks," *Sensors*, vol. 14, pp. 18625-18649, 2014.
- [37] W. de Vries, H. Veeger, C. Baten och F. van det Helm, Magnetic distortion in motion labs, implications for validating inertial, Elsevier, 2008.

- [38] D. Laidig, P. Müller och T. Seel, "Automatic anatomical calibration for IMUbased elbow angle measurement in disturbed magnetic fields," *Current Directions in Biomedical Engineering*, 2017.
- [39] J. Favrea, B. Jollesb, R. Aissaouic och K. Aminiana, "Ambulatory measurement of 3D knee joint angle," *Journal of Biomechanics*, vol. 41, pp. 1029-1035, 2008.
- [40] V. e. al, "Method for Estimating Three-Dimensional Knee rotation using using two imus," *Sensors*, 2017.
- [41] A. M. Sabatini, "Estimating Three-Dimensional Orientation of Human Body Parts by Inertial/Magnetic Sensing," *Sensors*, pp. 1489-1525, 2011.
- [42] R. Valenti, I. Dryanovski och J. Xiao, "Keeping a Good Attitude: A Quaternion-Based Orientation Filter for IMUs and MARGs," *Sensors*, pp. 19302-19330, 2015.
- [43] D. Q. Huynh, "Metrics for 3D Rotations: Comparison and Analysis," Springer, 2009.
- [44] L. Perumal, "Euler angles: conversion of arbitrary rotation sequences to specific rotation sequence," Wiley, 2013.
- [45] M. Arribas, A. Elipe och M. Palacios, "Quaternions and the rotation of a rigid body," *The international journal Celestial Mechanics and Dynamical Astronomy*, pp. 239-251, 2006.
- [46] <https://commons.wikimedia.org/wiki/File:Eulerangles.svg>, "Eulerangles". [USED 2018 02 20].
- [47] https://commons.wikimedia.org/wiki/File:Euler_AxisAngle.png, "Euler_AxisAngle". [USED 2018 02 20].
- [48] J. Qi, P. Yang, G. Min, O. Armft, F. Dong och L. Xu, "Advanced internet of things for personalised healthcare systems: A survey," *Pervasive and Mobile computing*, pp. 132-149, 2017.
- [49] S. Rodríguez-Valenzuela, J. A. Holgado-Terriza, J. M. Gutiérrez-Guerrero och J. L. Muros-Cobos, "Distributed Service-Based Approach for Sensor Data Fusion in IoT Environments," *Sensors*, 2014.
- [50] A. Marakhimov och J. Jo, "Consumer adaptation and infusion of wearable devices for healthcare," *Computers in Human Behavior*, pp. 135-148, 2017.
- [51] A. Rahmani, T. Nguyen, B. Negash, A. Anzanpour, I. Azimi, M. Jiang och P. Liljeberg, "Exploiting smart e-Health gateways at the edge of healthcare Internet-of-Things: A fog computing approach," *Future Generation Computer Systems*, vol. 78, pp. 641-658, 2018.

- [52] F. Abtahi, M. Forsman, F. Seoane, H. Teriö, C. Martinez, S. Aso, J. A. Diaz-Olivares, L. Yang, K. Lu, J. Eklund och K. Lindecrantz, "Big Data & Wearable Sensors Ensuring Safety and Health @Work," i *GLOBAL HEALTH 2017 : The Sixth International Conference on Global Health Challenges*, 2017.
- [53] A. Chaudhary, S. Peddoju och K. Kadarla, "Study of Internet-of-Things Messaging Protocols used for Exchanging Data with External Sources," i *2017 IEEE 14th International Conference on Mobile Ad Hoc and Sensor System*, 2017.
- [54] H.-L. Chang, C.-G. Wang, M.-T. Wu, M.-H. Tsai och C.-Y. Li, "Gateway-Assisted Retransmission for Lightweight and Reliable IoT Communication," *Sensors*, 2016.
- [55] N. Naik, "Choice of Effective Messaging Protocols for IoT Systems: MQTT, CoAP, AMQP and HTTP," i *Systems Engineering Symposium (ISSE), 2017 IEEE International*, 2017.
- [56] I. B. M. C. (IBM), "MQTT V3.1 Protocol Specification," 2010. [Online]. Available: <http://public.dhe.ibm.com/software/dw/webservices/ws-mqtt/mqtt-v3r1.html>. [USED 2018 02 20].
- [57] V. Abramova och J. Bernadino, "NoSQL Databases: MongoDB vs Cassandra," i *C3S2E '13 Proceedings of the International C* Conference on Computer Science and Software Engineering*, 2013.
- [58] J. Van der Veen, B. Vand der Waaij och R. Meijer, "Sensor Data Storage Performance: SQL or NoSQL, Physical or Virtual," i *2012 IEEE Fifth International Conference on Cloud Computing*, 2012.
- [59] Z. Goli-Malekabadi, M. Sargolzaei-Javan och M. Akbari, "An effective model for store and retrieve big health data in cloud computing," *Computer Methods and Programs in Biomedicine*, nr 132, pp. 75-82, 2016.
- [60] M. Patil, A. Hanni, C. Tejeshwar och P. Patil, "A qualitative analysis of the performance of MongoDB vs MySQL Database based on insertion and retrieval operations using a web/android application to explore Load Balancing - Sharding in MongoDB and its advantages," i *International conference on I-SMAC (IoT in Social, Mobile, Analytics and Cloud) (I-SMAC 2017)*, 2017.
- [61] A. Corbellini, C. Mateos, A. Zunino, D. Godoy och S. Schiaffino, "Persisting big-data: The NoSQL landscape," *Information Systems*, vol. 63, pp. 1-23, 2017.
- [62] N. Q. Mehmoor, R. Culmone och L. Mostarda, "Modeling temporal aspects of sensor data for MongoDB NoSQL database," *Journal of Big Data*, vol. 4, nr 8, 2017.
- [63] M. Skarman och J. Östelid, "Relationsdatabas eller NoSQL? En jämförelse mellan MSSQL och MongoDB," Karlstad Universitet, Karlstad, 2016.



LPMS-B2

LPMS Wireless Miniature Motion Sensor / IMU / AHRS with Bluetooth Connectivity

The LPMS-B2 is an innovative and high performance miniature wireless motion sensor. Based on Bluetooth technology, LPMS-B2 communicates with host systems like PCs, mobile devices etc. While maintaining high accuracy and quality, LPMS-B2 perfectly fits both machine and human motion measurements for size and cost sensitive applications.

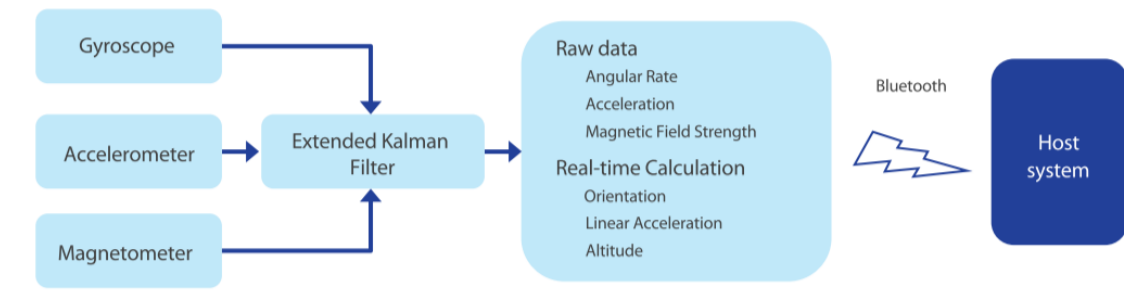


Key Features

- MEMS miniature inertial measurement unit (IMU)
- Integration of 3-axis gyroscope, accelerometer, magnetometer, temperature and barometric pressure sensor in one unit
- Real-time, on-device calculation of sensor orientation, linear acceleration and altitude
- Data output rates of up to 400Hz
- Wireless communication via Bluetooth 2 and Bluetooth LE (Low Energy / 4)
- Capability to record measurement data on device flash memory
- Control application and SDK for Windows, Linux and mobile platform (Android)

Applications

- Human motion capture
- Internet of Things (IoT) devices
- Sports performance evaluation
- Drone flight control



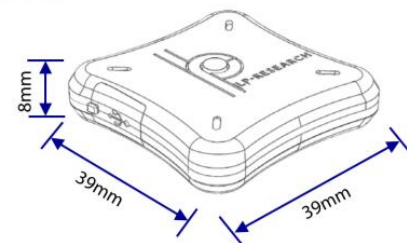
Sensor Specifications

	LPMS-B2	LPMS-B2 OEM
Size	39x39x8mm	16x31x4mm
Weight	12g	2g
Bluetooth	Bluetooth 2 / Low Energy (LE)	
Communication distance	< 20 m	
Orientation range	Roll: $\pm 180^\circ$; Pitch: $\pm 90^\circ$; Yaw: $\pm 180^\circ$	
Resolution	< 0.01°	
Accuracy	< 0.5° (static), < 2° RMS (dynamic)	
Accelerometer	3-axis, $\pm 2 / \pm 4 / \pm 8 / \pm 16$ g, 16 bits	
Gyroscope	3-axis, $\pm 125 / \pm 245 / \pm 500 / \pm 1000 / \pm 2000$ dps, 16 bits	
Magnetometer	3-axis, $\pm 4 / \pm 8 / \pm 12 / \pm 16$ gauss, 16 bits	
Pressure sensor	300-1100 hPa	
Data output format	Raw data / Euler angle / Quaternion	
Data output rate	up to 400Hz	
Power consumption	< 132 mW @ 3.3V	
Power supply	Lithium battery >6h (3.7 v@ 230mAh)	3.3-5.5V DC
Temperature range	-20 to +60°C	-40 to +80°C
Power Connector	Micro USB, Type B	Micro USB, Type B; SM02B-SURS-TF;
Software	C++ library for Windows, Java library for Android, LpmsControl software and Open Motion Analysis Toolkit (OpenMAT) for Windows.	

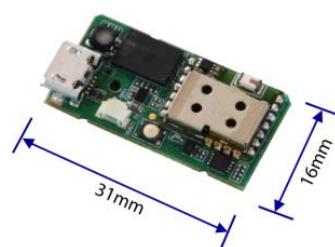


Mechanical Drawing

LPMS-B2:



LPMS-B2 OEM:

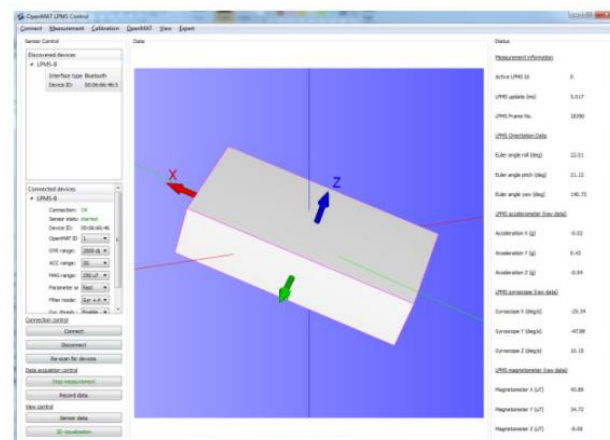


Package

- LPMS-B2 sensor x 1
- User guide card x 1
- Cable x 1
- Box x 1
- Warranty (1 year)



LpmsControl Utility Software



LP-RESEARCH CORPORATION
#303 Y-Flat, 1-11-15, Nishiazabu, Minato-ku, Tokyo, 106-0031 Japan
Tel: +81-3-6804-1610
Email: info@lp-research.com
Web: http://www.lp-research.com

Shimmer ECG & EMG Unit



INTRODUCTION

The ECG & EMG unit, previously also known as the ExG unit, provides a configurable digital front-end, optimized for the measurement of physiological signals, for example 5-lead ECG (Electrocardiography) and 2-channel EMG (Electromyography).

Compatible with the Shimmer3 platform, the ECG/EMG unit also boasts best data quality with integrated 10 DoF inertial sensing via accelerometer, gyroscope, magnetometer and altimeter, each with selectable range. The ECG/EMG unit also provides highly accurate and scientifically reliable raw data to allow complete control over capture and interpretation of sensed data in real-time.

PRODUCT OVERVIEW

While addressing the challenges of mobility, the ECG unit can record the pathway of electrical impulses through the heart muscle, and can be recorded on resting and ambulatory subjects.

When configured for EMG, the unit can also measure and record the electrical activity associated with muscle contractions, assess nerve conduction, muscle response in injured tissue, activation level, or can be used to analyse and measure the biomechanics of human movement.

KEY FEATURES

- Five-wire, four-channel ECG solution, measuring bipolar limb leads and user's choice of V1 - V6
- Measure two channels of EMG data with a common reference electrode
- Software configurable right-leg drive for common-mode interference rejection
- Software configurable amplifier gain
- Software configurable data rate
- Respiration demodulation capability on-chip
- Lead-off detection capability on-chip
- Test signal on-chip for validation purposes
- EEPROM storage device (on the ExG daughterboard) enables expansion board detection and identification, as well as 2032 bytes of data storage available to user

APPLICATIONS

The ECG/EMG unit is compatible with the Shimmer3 platform and can be applied to a variety of applications such as:

- Atrial fibrillation
- Premature ventricular contraction
- Heart function monitoring
- Abnormal rhythm detection and alert
- Biomechanics, muscle activity, gait and posture disturbance
- Fatigue analysis
- Sports technique, performance and medicine
- Neuro Rehabilitation
- Tremor Analysis
- Veterinary Science
- Orthopedics

Shimmer3 ECG & EMG Unit



TECHNICAL SPECIFICATIONS

Gain:	Software configurable (1, 2, 3, 4, 6, 8, 12)
Data Rate:	Software configurable (125, 250, 500, 1000, 2000, 4000, 8000 SPS)
Input Differential	Approx 800 mV (for gain = 6)
Dynamic Range:	
Bandwidth:	8.4 kHz
Ground:	Wilson Type Driven Ground
Input Protection:	ESD and RF/EMI filtering; Current limiting; inputs include defibrillation protection (survive only, not repeat)
Connections:	EMG: Input Ch1N, Input Ch1P, Input Ch2N, Input Ch2P, Reference (Ref) ECG: Input RA, Input LA, Input LL, Input Vx, Reference (RL) All Hospital-Grade 1mm Touchproof IEC/EN 60601-1 DIN42-802 jacks
Weight:	31 grams
Dimensions:	65 x 32 x 12 mm
EEPROM Memory:	2048 bytes

SHIMMER3 UNIT SPECIFICATIONS

Processing:	MSP 430 microcontroller (24MHz, 16Bit)
Communication:	Bluetooth – RN42, 802.15.4 radio – TI CC2420
Storage:	Integrated 8GB microSD card slot
Battery:	450mAh rechargeable Li-ion
Integrated 3 Axis Accel:	Freescale MMA7361
Accel Range:	+/- 1.5g – 6g

SUPPORTING SOFTWARE

Shimmer Consensys Software
ShimmerCapture
Shimmer 9DoF Calibration
ShimmerSensing LabVIEW Instrument Driver
Shimmer MATLAB Instrument Driver
Shimmer Java/Android API & Shimmer C#API
Shimmer Plot
Synchronisation of Data: Consensys Software
Multi Shimmer Sync for Android

© Copyright 2015 Shimmer
Specifications are subject to change without notice
S-S/ExG-v1.5



ECG MODULE SPECIFICATIONS

Five-wire, four-channel ECG solution, measuring bipolar limb leads
and user's choice of V1 - V6
Digital interface includes test signal generation for validation
purposes
Respiration demodulation from ECG data and lead-off detection

EMG MODULE SPECIFICATIONS

Two channels of EMG data
Digital interface includes test signal generation for validation
purposes

Shimmer International Offices:

Europe – Dublin, Ireland.
USA – Boston, MA.
Asia – Kuala Lumpur, Malaysia.

Web: www.ShimmerSensing.com
Email: info@ShimmerSensing.com

Appendix D: Additional test data

D1: First repetition of IMU dynamic test

Additional results from the first repetition of IMU dynamic test performed in 30, 60 120 and 180 BPM.

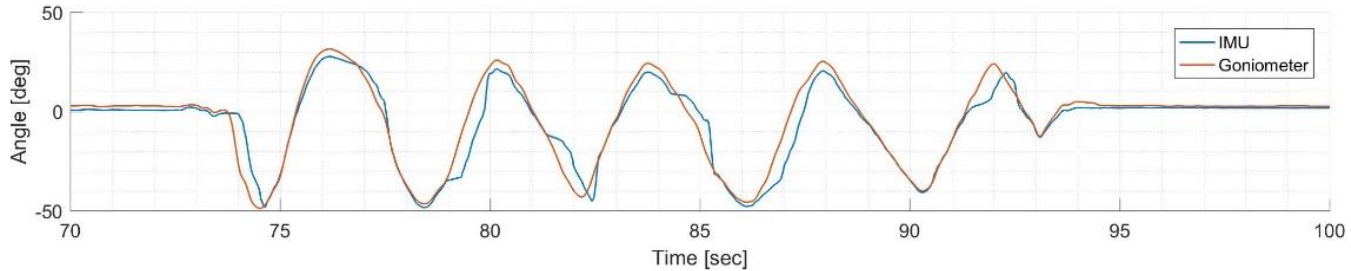


Figure D1.1: Flexion-extension angles measured with IMU:s (blue) and goniometers (red) for 30 BPM. Angle error in black.

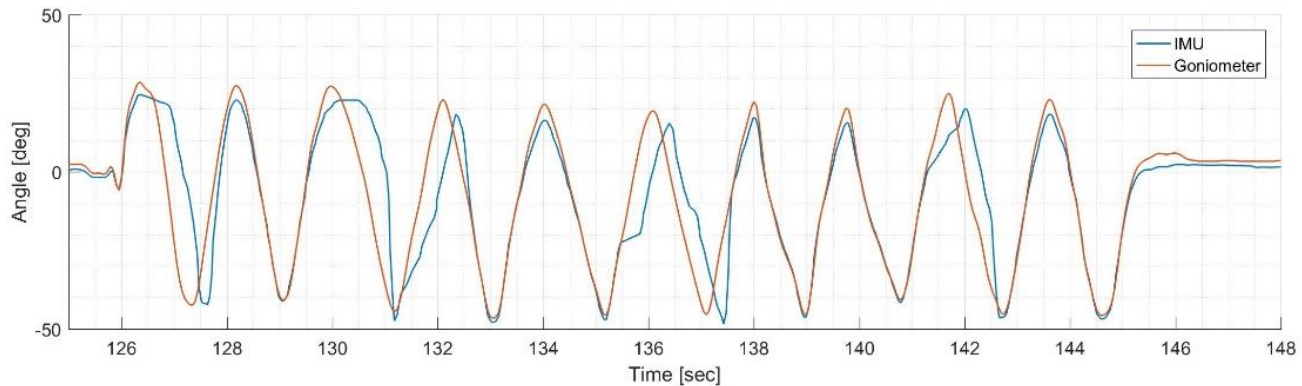


Figure D1.2: Flexion-extension angles measured with IMU:s (blue) and goniometers (red) for 60 BPM. Angle error in black.

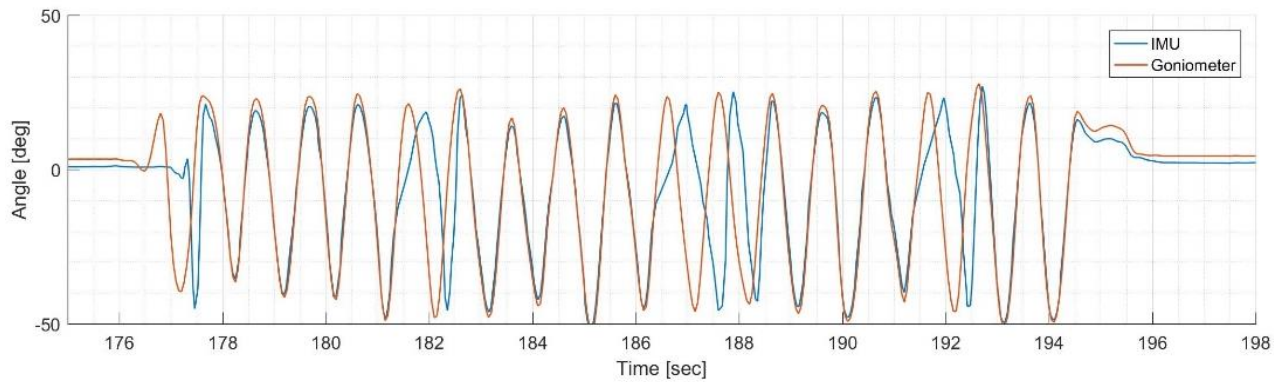


Figure D1.3: Flexion-extension angles measured with IMU:s (blue) and goniometers (red) for 120 BPM. Angle error in black.

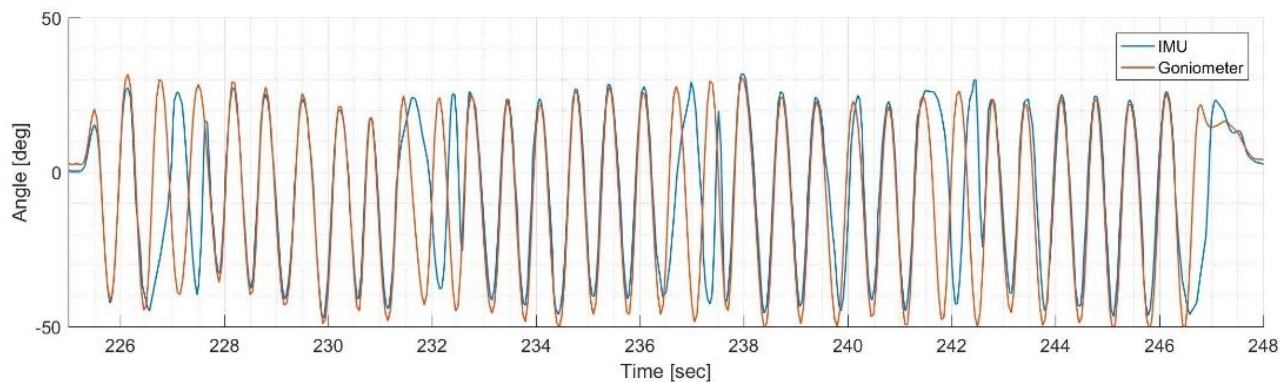


Figure D1.4: Flexion-extension angles measured with IMU:s (blue) and goniometers (red) for 180 BPM. Angle error in black.

Table D1.1: RMSE for angles and angular velocity's, compared to goniometer.

Test sequence	RMSE	
	Angle [°]	Angular velocity [°/sec]
30 BPM	8°	29
60 BPM	12°	55
120 BPM	17°	125
180 BPM	21°	180

D2: Second repetition of IMU dynamic test

Additional results from the second repetition of IMU dynamic test performed in 30, 60 120 and 180 BPM.

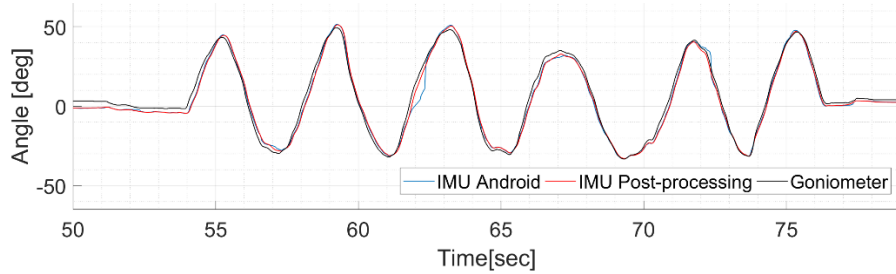


Figure D2.1: Flexion-extension angles measured with IMU:s (blue). Separate sampling and post-processing of IMU:s (red) and goniometer (black) for 30 BPM.

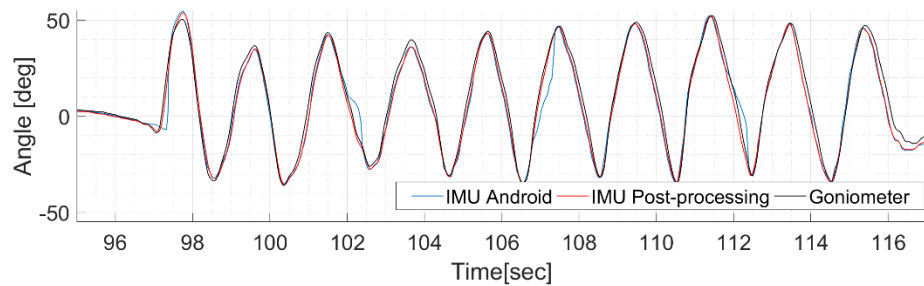


Figure D2.2: Flexion-extension angles measured with IMU:s (blue), separate sampling and post-processing of IMU:s (red) and goniometer (black) for 60 BPM.

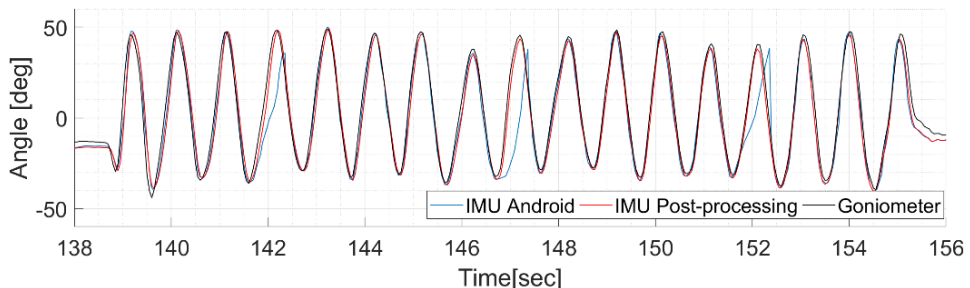


Figure D2.3: Flexion-extension angles measured with IMU:s (blue), separate sampling and post-processing of IMU:s (red) and goniometer (black) for 120 BPM.

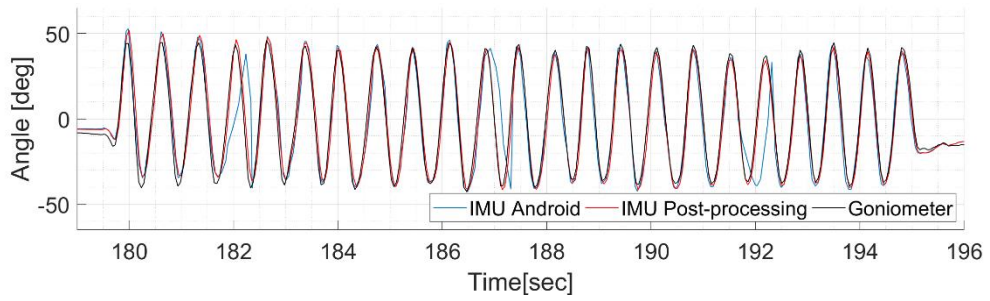


Figure D2.4: Flexion-extension angles measured with IMU:s (blue), separate sampling and post-processing of IMU:s (red) and goniometer (black) for 180 BPM.

D3: Bluetooth sample loss

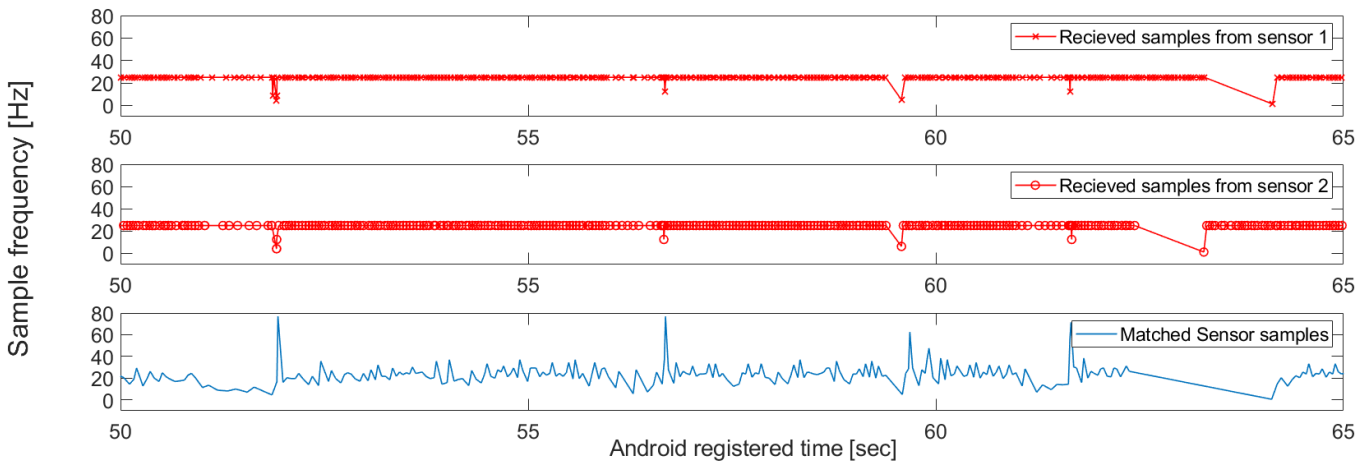


Figure D3: Bluetooth packet-losses.
Sampling frequency from the sample-pairing (blue) and independent sampling of the sensors (red).
Drops from 25-Hz line suggests Bluetooth-packages are lost.

D4: FIR-filter for angles

```
function y = Lpass(x)
%HPASS Filters input x and returns output y.

% MATLAB Code
% Generated by MATLAB(R) 9.2 and the DSP System Toolbox 9.4.
% Generated on: 05-Mar-2018 15:18:02

 %#codegen

% To generate C/C++ code from this function use the codegen command. Type
% 'help codegen' for more information.

persistent Hd;

if isempty(Hd)

    % The following code was used to design the filter coefficients:
    % % FIR Window Lowpass filter designed using the FIR1 function.
    %
    % % All frequency values are in Hz.
    % Fs = 20; % Sampling Frequency
    %
    % N      = 31;          % Order
    % Fc     = 5;           % Cutoff Frequency
    % flag   = 'scale';    % Sampling Flag
    %
    % % Create the window vector for the design algorithm.
    % win = blackman(N+1);
    %
    % % Calculate the coefficients using the FIR1 function.
    % b = fir1(N, Fc/(Fs/2), 'low', win, flag);

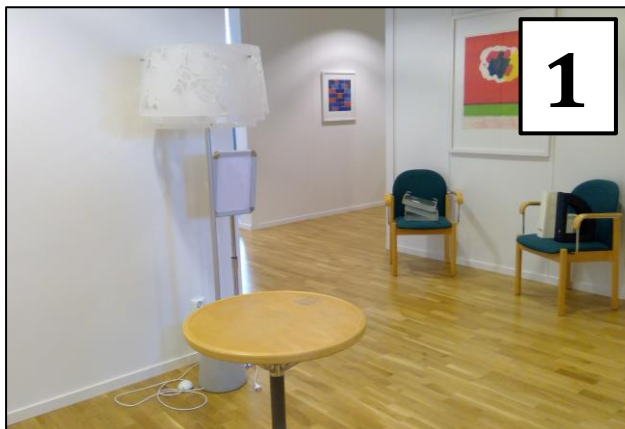
Hd = dsp.FIRFilter( ...
    'Numerator', [0 -5.82333046693299e-05 0.000260721291797632 ...
    0.000673456519917491 -0.00139865239852817 -0.00257836311618485 ...
    0.00439825403035122 0.00709511628134253 -0.0109754397743494 ...
    -0.0164604929940812 0.0241940942482038 0.0353109415298182 ...
    -0.0521835368043016 -0.0809791405480785 0.144454205113808 ...
    0.448247069924954 0.448247069924954 0.144454205113808 ...
    -0.0809791405480785 -0.0521835368043016 0.0353109415298182 ...
    0.0241940942482038 -0.0164604929940812 -0.0109754397743494 ...
    0.00709511628134253 0.00439825403035122 -0.00257836311618485 ...
    -0.00139865239852817 0.000673456519917491 0.000260721291797632 ...
    -5.82333046693299e-05 0]);

end

y = step(Hd,double(x));
```

D5: Magnetometer field environment test – Positions

Static positions used for test 2.1.3, result shown in part 3.1.2 (fig. 3.2 & 3.3)



Position 1: Horizontal on table

Position 2: Horizontal in bookshelf

Position 3: Horizontal on countertop

Position 4: Vertical (again seat back)

Position 5: Horizontal in chair

TRITA-CBH-GRU-2018:60